

IMAGING SOLAR CELLS
USING TERAHERTZ WAVES

A THESIS SUBMITTED TO
THE GRADUATE SCHOOL OF NATURAL AND APPLIED SCIENCES
OF
MIDDLE EAST TECHNICAL UNIVERSITY

BY

SEDA KAYRA

IN PARTIAL FULFILLMENT OF THE REQUIREMENTS
FOR
THE DEGREE OF MASTER OF SCIENCE
IN
PHYSICS

JANUARY 2011

Approval of the thesis:

IMAGING SOLAR CELLS WITH TERAHERTZ WAVES

Submitted by **SEDA KAYRA** in partial fulfillment of the requirements for the degree of **Master of Science in Physics Department, Middle East Technical University** by,

Prof. Dr. Canan Özgen
Dean, Graduate School of **Natural and Applied Sciences** _____

Prof. Dr. Sinan Bilikmen
Head of Department, **Physics** _____

Assist. Prof. Dr. Hakan Altan
Supervisor, **Physics Dept., METU** _____

Examining Committee Members:

Prof. Dr. Sinan Bilikmen
Physics Dept., METU _____

Assist. Prof. Dr. Hakan Altan
Physics Dept., METU _____

Prof. Dr. Raşit Turan
Physics Dept., METU _____

Assist. Prof. Dr. Okan Esentürk
Chemistry Dept., METU _____

Dr. Halil Berberoğlu
Physics Dept., METU _____

Date: January 27th, 2011

I hereby declare that all information in this document has been obtained and presented in accordance with academic rules and ethical conduct. I also declare that, as required by these rules and conduct, I have fully cited and referenced all material and results that are not original to this work.

Name, Last name: Seda KAYRA

Signature:

ABSTRACT

IMAGING SOLAR CELLS WITH TERAHERTZ WAVES

Kayra, Seda

M.Sc., Department of Physics

Supervisor: Assist. Prof. Dr. Hakan Altan

January 2011, 77 pages

In this thesis, Terahertz Time-Domain spectroscopy (THz-TDS) was used in order to measure the electrical properties of silicon solar cells. The advantage of THz-TDS is that it allows us to measure the electrical properties without electrical contacts. In order to perform these measurements, a reflection based system was constructed and the changes in the peak amplitude in the time-domain under a, 450mW 808 nm continuous wave laser source were measured. The solar cell that was used in this thesis was manufactured in Middle East Technical University Microelectromechanical Systems (METU-MEMS) research laboratories located in Ankara, Turkey. The solar cell that we used in the measurements had a thickness of 0.45 mm and was produced on a single silicon crystal in <100> direction. It is made up of a p-type base and n-type emitter to create p-n junction. Also, it has a Si₄N₃ AR coating and Al back contacts on it. To compare the THz measurements to that of

electrical measurements, some electrical contact measurements were performed on the solar cell under laser illumination. By using these measurements, the energy conversion efficiency and the quantum efficiency of the solar cell were calculated and measured as 3.44 % and 7%, respectively under the 450mW, 808nm illumination on a specific area of the cell. The results that were obtained from the electrical measurements were compared with the THz results. We found that in order to understand the efficiency of the solar cell using THz-TDRS, a more comprehensive study needs to be done where the changes in the reflection of the THz radiation under different excitation powers and different configurations of the system need to be studied.

Keywords: Terahertz, silicon solar cell, THz-TDRS, efficiency, electrical measurements

ÖZ

TERAHERTZ DALGALARINI KULLANARAK GÜNEŞ GÖZELERİNİ GÖRÜNTÜLEME

Kayra, Seda

Yüksek Lisans, Fizik Bölümü

Tez Yöneticisi: Yrd. Doç. Dr. Hakan Altan

Ocak 2011, 77 sayfa

Bu çalışmada, silikon güneş gözelerinin elektriksel özelliklerini ölçmek için Zamana Dayalı THz Spektroskopisi (THz-TDS) kullanılmıştır. Bu spektroskopinin kullanılmasındaki avantaj, güneş gözesine elektrik kontakt uygulamadan elektriksel özelliklerini ölçebilmemize izin vermektir. Bu ölçümleri yapabilmek için yansıma geometrisine sahip Zamana Dayalı THz Spektroskopisi kullanılmıştır ve 808 nm sürekli dalga boyuna, 450 mW güce sahip bir ışık kaynağı altında THz sinyalinin büyüklüğü ölçülmüştür. Bu çalışmada kullanılan güneş gözesi, Ankara, Türkiye’de yer alan Orta Doğu Teknik Üniversitesi Mikroelektromekanikal Sistemler (ODTÜ MEMS) araştırma laboratuvarı tarafından üretilmiştir. Ölçümlerde kullanılan bu güneş gözesi 0.45 mm kalınlığa sahip olup $\langle 100 \rangle$ yönünde kesilmiş silikon kristalden

üretimiştir ve p-n eklemi oluşturmak için p-tipi baz ve n-tipi emitere sahiptir. Ayrıca, üzerine yansıma önleyici Si_3N_4 kaplanan silikon güneş gözesine Al kontaklar yapılmıştır. Güneş gözesinden alınan THz ölçümlerini elektriksel ölçümler ile karşılaştırmak için lazer kaynağı altında elektriksel kontakt ölçümleri alınmıştır. Bu ölçümleri kullanarak, 808 nm dalga boyuna ve 450 mW güce sahip lazer kaynağı güneş gözesinin belirli bir alanını aydınlatarak, verimliliği 3.44 % ve kuantum verimliliği ise 7 % olarak hesaplanmış ve ölçülmüştür. Elektriksel ölçümlerden elde edilen bu sonuçlar THz ölçümlerinden elde edilen sonuçlar ile karşılaştırılmıştır. Zamana Dayalı THz Yansıma Spektroskopisi kullanılarak güneş gözesi verimliliğini anlayabilmek için daha kapsamlı bir çalışma yapılması gerekmektedir. Böylelikle, farklı güçte ışık kaynağı kullanarak ve sisteme farklı konfigürasyonlar uygulanarak THz dalgalarının yansıma profillerindeki değişiklikler incelenebilecektir.

Anahtar kelimeler: Terahertz, silikon güneş gözesi, THz-TDRS, verimlilik, elektriksel ölçümler

To my family

ACKNOWLEDGEMENTS

I would like to express my deep gratitude and thanks to my supervisor Assist. Prof. Dr. Hakan Altan for his endless patience, understanding, cooperation and support throughout this study.

I would also like to present my sincere thanks to Zeynep Türkşen for her precious help with the experiments, fruitful discussions and valuable friendship. I am indebted to Prof. Dr. Raşit Turan and his Gunam workers; Fırat Es, Olgu Demircioğlu, Mehmet Karaman for their scientific contributions to this study.

Special thanks go to all of my family for their continuous support and love at the each stage of my educational life. Very special thanks go to my husband Hasan Hüseyin Güllü whose love, steadfast confidence and constant encouragement. Without them this work would never have come into existence.

Moreover, this thesis project was supported by The Scientific and Technological Research Council of Turkey (TÜBİTAK) grant number 107T742.

TABLE OF CONTENTS

ABSTRACT	iv
ÖZ	vi
ACKNOWLEDGEMENTS	ix
LIST OF TABLES	xii
LIST OF FIGURES	xiii
CHAPTERS	1
1. INTRODUCTION	1
2. PRINCIPLES OF TERAHERTZ SPECTROSCOPY	8
2.1. TERAHERTZ TIME DOMAIN SPECTROSCOPY (THz-TDS)	8
2.2. TERAHERTZ GENERATION	11
2.2.1. Generation of THz Radiation by Using Photoconductive Antenna.....	11
2.2.2. Generation of THz Radiation by Using Electro-Optic Crystal.....	16
2.3. TERAHERTZ DETECTION.....	18
2.3.1. Detection of THz Radiation by Using Photoconductive Antenna.....	18
2.3.2. Detection of THz Radiation by Using Electro-Optic Crystal.....	19
2.4. THz TIME DOMAIN REFLECTION SPECTROSCOPY (THz-TDRS)	21
2.4.1. System Design and Optical Components.....	23
2.5. MEASUREMENTS ON THE SILICON WAFER	33
3. OPERATION PRINCIPLES OF SOLAR CELL	37
3.1. SEMICONDUCTOR MATERIAL PROPERTIES	38
3.1.1. Structure of Semiconductors.....	38
3.1.2. Intrinsic Carrier Concentration	41
3.1.3. Absorption of Light	42

3.1.4. Generation Rate	44
3.1.5. Types of Recombination Process.....	45
3.1.6. Lifetime.....	46
3.1.7. Diffusion	47
3.1.8. P-N Junction	47
3.2. SOLAR CELL OPERATION	50
3.2.1. Structure of Solar Cell	50
3.2.2. Quantum Efficiency (Q.E.).....	52
3.2.3. Spectral Response	53
3.2.4. Photovoltaic Effect	53
3.3. CHARACTERIZATION OF A SOLAR CELL.....	54
3.3.1. Parameters of a Solar Cell	54
3.3.1.1. IV Curve.....	54
3.3.1.2. Short Circuit Current.....	56
3.3.1.3. Open Circuit Voltage	57
3.3.1.4. Fill Factor	58
3.3.1.5. Solar Cell Efficiency	59
3.4. EFFECT OF TEMPERATURE	60
3.5. DISCUSSION.....	60
4. MEASUREMENTS OF THE SOLAR CELL	62
4.1 THz MEASUREMENTS.....	62
4.1.1. Experimental Procedure.....	62
4.1.2. Measurements of the Solar Cell by Using THz-TDRS.....	65
4.2. ELECTRICAL MEASUREMENTS	67
4.2.1. Experimental Procedure.....	67
4.2.2. Efficiency Calculation of the Solar Cell by Using Electrical Measurements	70
5. CONCLUSION	71
REFERENCES.....	74

LIST OF TABLES

TABLES:

Table 2.1: Characteristics of photoconductive materials	14
Table 2.2: Optical wavelengths for velocity-matching in zinc blende crystals	18
Table 2.3: Specifications of Ultrafast mode-locked Erbium doped fiber laser	24
Table 2.4: Electrical parameters of photoconductive antenna	25
Table 2.5: Optical Parameters of photoconductive antenna.....	25
Table 4.1: Peak-to-Peak voltages of THz Measurements with and without illumination.....	65

LIST OF FIGURES

FIGURES:

Figure 1.1: The electromagnetic spectrum from radio waves to X-rays with electronics and optics region.....	2
Figure 2.1: Top-view of the photoconductive antenna [39].....	12
Figure 2.2: Schematic view of the photoconductive antenna	13
Table 2.1: Characteristics of photoconductive materials [1]	14
Table 2.2: Optical wavelengths for velocity-matching in zinc blende crystals	18
Figure 2.3: The directions of the optical and THz pulses for EO sampling [1].....	20
Figure 2.4: THz Time Domain Transmission Spectroscopy experimental setup	22
Figure 2.5: View of the photoconductive antenna in two different aspects [19]	24
Table 2.4: Electrical parameters of photoconductive antenna [39].....	25
Table 2.5: Optical Parameters of photoconductive antenna [39].....	25
Figure 2.7: THz waveform before placing the reflectance mirrors and TPX lenses..	28
Figure 2.8: Power spectrum of the THz waveform before placing the reflectance mirrors and TPX lenses.....	29
Figure 2.9: THz-TDRS experimental setup with paraboloidal reflectors and TPX lenses.....	30
Figure 2.10: THz waveform after placing the reflectance mirrors and TPX lenses ..	31
Figure 2.11: Power spectrum of the THz waveform after placing the reflectance mirrors and TPX lenses.....	32
Figure 2.12: THz waveform of reference mirror	34
Figure 2.13: THz waveform of the silicon wafer.....	34
Figure 2.14: Spectral response curve of silicon [36].....	35
Figure 2.15: Comparison between the THz waveforms in both measurements	36
Figure 3.1: Allowed states that are occupied by electrons in (a) a metal, (b) an insulator, (c) a semiconductor. Fermi level is used to describe the top of the	

collection of electron energy level at absolute zero. It gives information about the probability of occupation of an electron in a given state [26].	39
Figure 3.2: Band Diagram of a semiconductor [35]	39
Figure 3.3: Energy-crystal momentum relations for a (a) direct-band-gap (b) indirect-band-gap semiconductor [30]	41
Figure 3.4: Radiative (Band-to-Band) Recombination	45
Figure 3.5: Auger Recombination [28]	46
Figure 3.6: P-N junction Diode Structure [32]	49
Figure 3.7: Solar Cell Structure	51
Figure 3.8: Quantum Efficiency of a silicon solar cell [32]	52
Figure 3.9: Without any illumination, a solar cell has the same electrical characteristics with a diode.	55
Figure 3.10: The incident light on the solar cell causes the shifting of the IV curve to the fourth quadrant.	56
Figure 3.11: As the intensity of the incident light on the solar cell increases, the amount of the shift of the curve becomes greater	56
Figure 3.12: Typical IV Curve	59
Figure 3.13: Single crystal silicon <100> solar cell.	61
Figure 4.1: Experimental set-up with the addition of Diode Laser	64
Figure 4.2: The comparison of THz profiles of the solar cell	65
Figure 4.3: IV Curve under dark field and illumination with THz radiation only	69
Figure 4.4: IV Curve under dark field and illumination with 808 nm laser only	70
Figure 4.5: IV Curve under dark field and illumination with 808 nm laser and THz radiation	70

CHAPTER 1

INTRODUCTION

Terahertz (THz) spectroscopy is defined as the detection and the analysis of the interaction of light in the THz frequency range with molecules, atoms and other solid-state materials. Until the late 1980's, this has been a newly developing area since the generation and the detection of light in THz frequencies were difficult [1]. Because of this difficulty in the methods of the generation and the detection, the region between 'electronics' and 'photonics' has been referred to as the 'THz gap' [2]. After the advent of generation and detection of THz pulses by using photoconductive antennas and optical rectification techniques, spectroscopy in THz region has become possible. In recent years, THz technology has become very important as new generation and detection techniques have been explored. These methods which rely on frequency conversion are generally more reliable, cheaper compared to older techniques and simpler to construct [3, 4]. Using nonlinear and linear optics, one of the most popular methods among many far-infrared spectroscopy techniques has been Terahertz Time-Domain Spectroscopy (THz-TDS). Since THz-TDS systems have broad bandwidth and high signal-to-noise ratio, it is a preferred technology for observing different systems [5].

After this technological development, this technique has been used for time-resolved studies of polar and non-polar liquids [6], solid-state materials [7] and biological media [8]. THz frequency range spans a significant portion of the electromagnetic spectrum. The THz region lies between the mid-infrared and the millimeter/microwave frequency range. The frequency of 1 THz corresponds to photon energy of 4.1 meV, a wavelength of 300 μm or 0.3 mm, to a wavenumber of

33 cm^{-1} , 1 ps and a temperature of 48 K . Therefore, THz fields have wavelengths extending from 3 mm (0.1 THz or 100 GHz) up to $30 \text{ }\mu\text{m}$ (10 THz) [9]. The location of the THz field in the electromagnetic spectrum is a mixture of both optical and electronic domains which is used for THz field generation, detection and processing.

Each wavelength and frequency region of the electromagnetic spectrum is shown below in the figure 1.1. According to this schematic illustration, the regions of electronics and optics are shown. Since microwave wavelengths are too long and optical wavelengths are too short when compared to THz field wavelengths, both optical and microwave techniques are not directly used in the THz range [10].

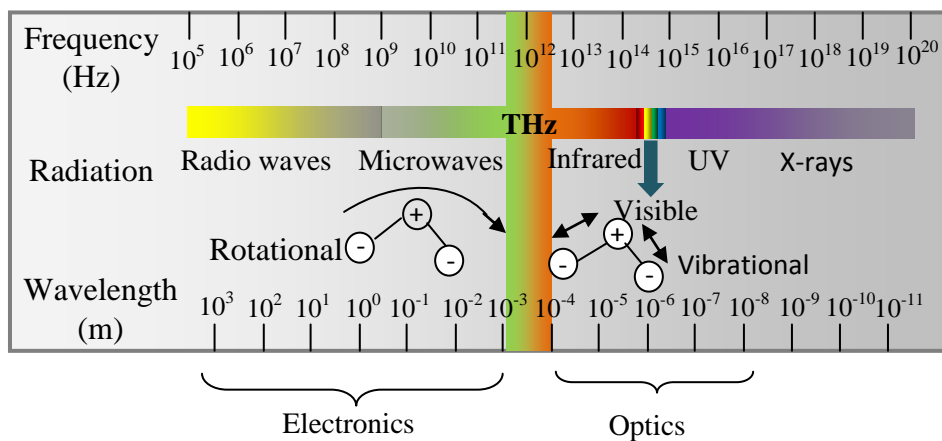


Figure 1.1: The electromagnetic spectrum from radio waves to X-rays with electronics and optics region.

Furthermore, most of the rotational frequencies lie in the microwave band; however, molecules which has less mass have higher rotational frequencies; therefore, light molecules have THz resonances. In addition, heavy molecules including biological molecules have broad resonances at THz frequencies.

There are many advantages of using THz waves in many applications. One of the advantages of THz radiation is that in this range, wavelengths are long enough so, they can penetrate non-polar, non-metallic materials. However, THz radiation is still short enough so, they can be used with optical components to form an image [9]. Moreover, the other advantage of the THz spectroscopy is that transient electric field is measured and therefore, the constituent elements of the pulse which are the amplitude and phase that have connection with the absorption coefficient and the refractive index of the sample are determined [12, 13].

The interest in THz range gained much attention in the early 1960's when researchers gave importance in the THz region of the electromagnetic spectrum [13]. In these years, there were few studies for generation and detection of THz radiation. At this time, the most critical problem was that THz beams could not propagate over long distances due to water absorption [14]. Following the 1970's, scientists contributed knowledge gained from microwave and optical techniques into THz studies. K. H. Yang et al. produced THz radiation by using nonlinear frequency conversion with an ultrafast laser [13, 15]. This was the beginning of the new era and this was followed by generating THz radiation by using optical rectification of short pulses as a different method by Y. R. Shen [16] in 1976. By the late 1980's, as the ultrafast lasers with femtosecond pulse durations became common, the techniques of generating THz radiation improved. Auston and Cheung [17] developed the first THz-TDS system at AT&T Bell Laboratories in 1985. With this technique, many methods were made in the generation and detection of THz radiation. In 1988, Peter Smith et al. [18] generated and detected THz radiation by using photoconducting antennas between 100 GHz and 2 THz. In 1989, Van Exter, Fattering, and Grischkowsky used photoconducting antennas in THz systems and showed that by using these devices, THz systems can be regarded as spectroscopic tools. In 1993, another method was improved to obtain THz radiation with narrow bandwidth by photo-mixing two lasers operating at different frequencies. After two years in 1995, free-space electro-optic sensing was developed by Wu and Zhang which provided broader detection bandwidths [19]. Again in the same year, the application in imaging by using THz-TDS was first reported by Hu and Nuss [20].

Moreover, THz waves are used in many applications. With developing technologies in electronics and photonics, THz technology has become a vital demand for security, medicine, communications and electronics as well as manufacturing where evaluating materials during and after production is an important step in order to satisfy the quality standards. In pharmaceutical applications, the structural map of a tablet can be viewed by THz imaging without giving any harm to the product. Important information, such as uniformity of ingredients and defects during or after the steps of the fabrication can be obtained [21]. Furthermore, studies in THz radiation have become a significant topic in astronomy since the THz range in the electromagnetic spectrum covers one half of the radiance of the observable universe. In biological science applications, due to the motion of groups of molecules, THz radiation interacts with matter and this provides the possibility of investigating a large portion of biological processes such as distinguishing one type of protein from another by using THz spectroscopy as well as a relatively large numbers of specific chemical substances [21].

THz radiation has broader usage areas relative to the other portions in the electromagnetic spectrum. Recent developments show that images of many kinds of materials can be taken by THz techniques. Materials which are opaque to THz waves such as metallic surfaces are studied upon reflection; however, most materials are transparent to THz radiation in some degree [22]. Therefore, THz reflection Spectroscopy is needed to measure opaque samples.

Furthermore, THz technology has many applications in semiconductors, composite materials and as we will show in this thesis, solar cells since THz spectroscopy provides structural information and can reveal defects if any in them [21]. THz portion of the electromagnetic spectrum is very suitable in order to characterize semiconductors since the collision frequency and the plasma frequency in these materials lie in the THz frequency range of the electromagnetic spectrum. These properties were successfully characterized first by Ohba and Ikawa [23, 24].

THz spectroscopy is an effective method to characterize Silicon (Si) based materials and structures. By using THz-TDS, plasma frequency has been studied for n-type

and p-type silicon. These experiments are done by comparing and analyzing THz waves reflected from the semiconductors and the reference mirror [25].

With the depletion of energy sources and the increase in the energy demands for the future, photovoltaic conversion of solar energy to electrical energy is one of the most promising developing techniques to solve this problem. The safety of the environment is not affected during the process of solar energy conversion by photonic devices and there is no impact on the contamination of nature. Therefore, this growing interest in photovoltaic conversion is leading the research and fabrication of these devices for future needs. In order to develop new technologies and improve the production methods and applications, research and application centers are being built. At METU in Physics Department, one of these centers named The Center for Solar Energy Research and Applications (GUNAM) has been founded to improve the solar energy technology and fabricate photovoltaic devices at a reasonable price.

The origin of the discovery of the solar cells can be traced back 140 years, to when the problems with resources arose. Since then, scientists have tried to find renewable and alternative energy sources directly to produce fuels and electricity [26]. Recently, researchers have again focused on solar technology and learned to use materials to create solar energy to electricity converters. One of the technologies is to use photovoltaic solar cells which convert the incoming solar radiation directly into electricity [27].

The history behind solar energy power began in 1839 when Becquerel discovered that when light was shone on an electrode in an electrolyte solution, a photovoltage was observed [27]. Then, Adams and Day reported a similar effect in the solid material selenium in 1877 [28]. As a result of focusing studies on photovoltaic effects on selenium, selenium photovoltaic cells were developed. Solar conversion efficiency, which is a parameter of a solar cell and determines the electrical power that a cell can produce, reached about 1% with the selenium cell by directly converting sunlight into electricity [29]. However, the modern era for the photovoltaics began with Chapin in 1954 by improving the solar conversion efficiency to 6% for a silicon single crystal cell [28, 30]. In 1958, efficiency of the

silicon cell had reached to 14%. Since silicon is the cheapest and the most abundant element available on earth, the usage of this element in solar cells has increased. In today's technology, silicon is used in different forms like single-crystalline, amorphous and polycrystalline for the solar cell fabrication. However, single-crystalline silicon structures are the most widely used commercially and have become the main focus of laboratory research and development [31]. After the mid 1980's, there has been a significant increase in the efficiencies of solar cells that are produced in laboratory conditions. With the best possible laboratory conditions, experiments show that the efficiency of the single crystal silicon solar cell can reach 24.7% [32]. However, these solar cells produced in the laboratory are much more expensive compared to commercial productions. The efficiencies of solar cells that generally occupy a large-area and can be mass produced for industrial purposes are much lower and is generally below 20% [33].

THz spectroscopy can be used for solar cell research to study ultrafast carrier dynamics in various types of semiconductors. Frequency dependent response can be obtained from the interaction of the THz field with charge carriers and gives information on the nature of carrier conductivity in a material [34]. Moreover, mobility, carrier density and the existence of plasma oscillations can be estimated by THz spectroscopy [32,34]. Therefore, in photovoltaic applications, in order to investigate the fundamental properties of a wide range of semiconductors, THz spectroscopy can be used.

In this thesis, THz Time Domain Reflection Spectroscopy (THz-TDRS) driven by an ultrafast laser source is constructed by using photoconductive antenna for the generation and electro-optic crystal for the detection. In chapter 2, brief information of THz-TDRS is given. Generation and detection methods are discussed. Moreover, an external 808 nm Diode Laser source is used in order to illuminate the samples. By using this reflection spectroscopy, two different THz profiles are obtained from an un-doped silicon wafer with and without a diode laser as a pump source and emphasized on this difference. In chapter 3, a brief theoretical background about the operation of a solar cell is discussed. The description of the solar cell that is used in this thesis is given. In chapter 4, the procedure of THz measurements for the solar

cell is explained and external quantum efficiency of the solar cell is calculated. Then, electrical measurement technique is used for the efficiency calculation of the solar cell in order to compare with the THz measurements. IV curves of the solar cell in the dark and under illumination are obtained by using electrical measurement technique. External quantum efficiencies and energy conversion efficiency of the solar cell is calculated. The relationship between the results of THz measurements of the solar cell and the efficiency calculations from the electrical measurements are discussed. In the last chapter, a brief summary about this thesis is done.

CHAPTER 2

PRINCIPLES OF TERAHERTZ SPECTROSCOPY

In this chapter, working principle of the pulsed THz Time Domain Spectroscopy (THz-TDS) will be explained by discussing the most popular generation and detection methods which are based on photoconductive antenna (PCA) and nonlinear electro-optic (EO) crystal. Then, the THz-TDRS will be introduced as a basic experimental configuration for the work in this thesis.

2.1. TERAHERTZ TIME DOMAIN SPECTROSCOPY (THz-TDS)

THz-TDS is a technique to obtain spectroscopic analysis in time domain and in frequency domain after Fourier transform. One of the most important properties of THz pulses is that THz spectroscopy measures not only the intensity but also the electric field of the pulse [1]. For the electric field vector, a general solution to the wave equation is

$$\tilde{E}_{THz}(\vec{r}, t) = \tilde{E}_0 \exp i(\vec{k} \cdot \vec{r} - \omega t + \varphi) \quad (2.1)$$

where \tilde{E}_{THz} is the complex form of electric field of THz waves, \vec{k} is the wave vector, ω is the angular frequency, and φ is the phase angle.

Moreover, amplitude and phase of the components of THz pulse are obtained by applying Fourier Transform to the electric field.

$$\tilde{E}(z, \omega) = \frac{1}{2\pi} \int_{-\infty}^{\infty} E(z, t) e^{-i\omega t} dt \quad (2.2)$$

Here, in this equation $\tilde{E}(z, \omega)$ is the complex field amplitude, $E(z, t)$ is the experimentally obtained electric field of THz pulse in the time domain and ω is the angular frequency. The relation between the intensity, I and the electric field, E can be written as:

$$I = \frac{1}{2} \sqrt{\frac{\mu_0}{\varepsilon}} E E^* \quad (2.3)$$

where I is the intensity, μ_0 is the vacuum permeability, ε is the permittivity, E and E^* are the electric field and complex conjugate of electric field of THz wave.

Intensity measurement does not contain phase information, whereas, phase information can be obtained from the electric field of the THz pulse. Therefore, it is more practical than the conventional Fourier Transform Infrared Spectroscopy (FTIR) that measures only intensity. The other advantage of this spectroscopy is the determination of real and imaginary parts of refractive index without making calculations using Kramers-Kronig relations [2, 3]. Applications with this type of spectroscopy can be carried out either in reflection or transmission geometry. Another similarity between THz and optical pulses is the result of the change in the phase as phase shifts when passing through or reflecting off materials which changes the pulse shape. Little phase changes cause significant re-shaping in THz pulses like inversion of the pulse [4].

Refractive index is a complex form and composed of real and imaginary parts and it can be shown as

$$\tilde{n}(\omega) = n_r(\omega) + i n_i(\omega) \quad (2.4)$$

where \tilde{n} is the complex form, n_r is the real part and n_i is the imaginary part of the refractive index. Also, the relation between the wave vector and the complex refractive index can be written as

$$k(\omega) = \frac{\nu \tilde{n}(\omega)}{c} \quad (2.5)$$

Here, ν is the frequency, $\tilde{n}(\omega)$ is the complex refractive index and c is the speed of light. Moreover, the imaginary part of the refractive index is calculated by using the absorption coefficient from the relation below.

$$\alpha(\omega) = \frac{2\omega n_i(\omega)}{c} \quad (2.6)$$

where $\alpha(\omega)$ is the absorption coefficient, n_i is the imaginary part of the refractive index and c is the speed of light.

The electric field obtained from the Fourier transform can be represented as

$$E(\omega) = |E(\omega)| e^{i\varphi(\omega)} \quad (2.7)$$

where $E(\omega)$ is the electric field vector, $|E(\omega)|$ is the amplitude of the electric field and $\varphi(\omega)$ is the phase of the electric field. The real part of the refractive index and the absorption coefficient of the material that is observed can be obtained from the Fourier transformed data. Then, the real part of the refractive index can be written as

$$n_r = \frac{1}{kl} (\varphi(\omega, l) - \varphi(\omega)) \quad (2.8)$$

where l is the length of the sample, k is the wave vector, $\varphi(\omega, l)$ and $\varphi(\omega)$ are the phase of the sample and reference pulse respectively. As shown in the above equation, the absorption coefficient is related to the imaginary part of the refractive index, so the formula becomes

$$\alpha(\omega) = \frac{\frac{2\omega}{kl} \left(\ln \left(\frac{E(\omega, l)}{E(\omega)} \right) \right)}{c} \quad (2.9)$$

The imaginary part of the refractive index is calculated from the ratio of the sample and reference electric field magnitudes.

$$n_i = \frac{1}{kl} \left(\ln \left(\frac{E(\omega, l)}{E(\omega)} \right) \right) \quad (2.10)$$

2.2. TERAHERTZ GENERATION

There are several ways to generate the pulsed THz radiation such as optical rectification, charge transfer and current surge [5]. On the other hand, photoconductive antenna (PCA), electro-optic (EO) crystals and bolometers are the basic detectors for pulsed THz radiation. Among them, the most widely-used methods to study and measure pulsed THz radiation are photoconductive antennas (photoconductive switch) and optical rectification (non-linear generation via difference frequency mixing). Both techniques use ultrafast lasers. These lasers are very useful in order to study the ultrafast phenomena in a subpicosecond time scale. Ultrafast lasers have short pulse duration. This property makes the intensity of the peak considerably high since all the energy of the optical pulse is focused on the short time period. Then, these short and high intensity pulses results in the change of the optical properties of the material.

2.2.1. Generation of THz Radiation by Using Photoconductive Antenna

PC antennas are the most common emitters and detectors used in THz-TDS systems. A PCA is a device based on a semiconductor that shows an increase in the electrical conductivity as it interacts with light. In this device, interactions between optical pulse (visible pulse from ultrafast laser) and the semiconductor material in a femtosecond time scale cause generation and detection of THz pulses [6, 7].

The general aim for generation of THz radiation is optical excitation in a semiconductor and changing the conductivity of the material.

In the construction of a PCA, two electrical contact pads and a highly resistive semiconductor thin film are used. A dipole antenna and a coplanar transmission line which connects the dipole antenna to the contact pads are also located on the

semiconductor substrate. Moreover, the antenna has a small gap about a few μm at its center. The basic structure of the photoconductive antenna is shown in the figure 2.1 below.

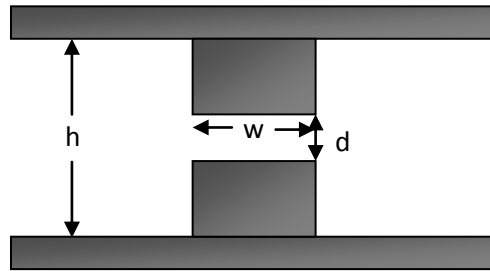


Figure 2.1: Top-view of the photoconductive antenna [39]

The length of the antenna denoted by h varies from 10 to 200 μm and the size of the center gap is related with the diameter of the optical pulse that is focused onto the gap [9, 10]. When there is no optical pulse incident, these types of antenna structures have dark resistances on the order of some mega ohms. The resistance of the antenna gap is expressed as $R(t) = w/\sigma(t)A$, where A is the cross-sectional area which is approximately $2d\alpha$ and d is much larger than the absorption depth and σ is the conductivity.

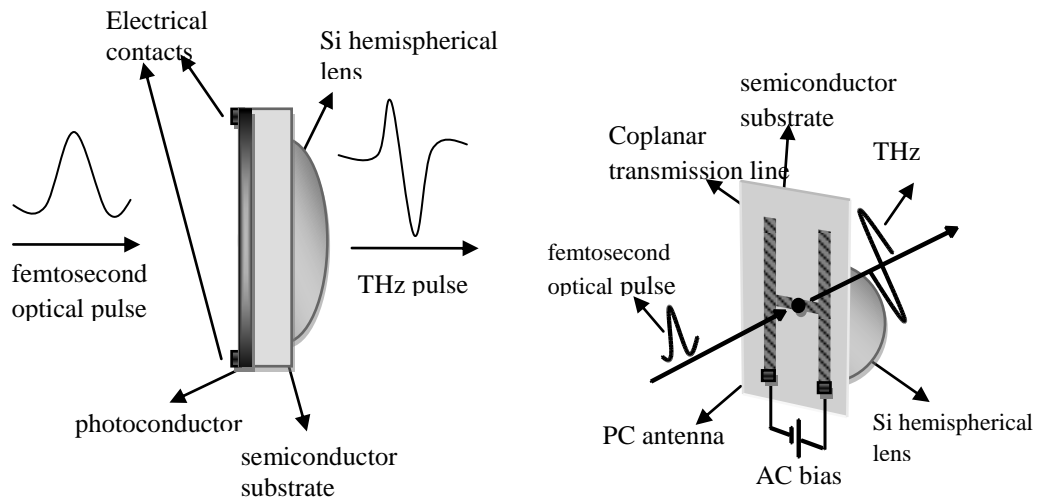


Figure 2.2: Schematic view of the photoconductive antenna

The basic principle of generation of THz radiation from PCA relies on the illumination of the photoconductive gap by a femtosecond laser pulse where the photon energy equals to or greater than the band gap energy of the semiconductor material [11].

Most widely used material in the antenna for THz waves is low-temperature grown GaAs (LT-GaAs) due to its perfect properties such as short carrier lifetime, high carrier mobility and high breakdown voltage or high resistivity. Breakdown voltage limits the high radiation power. Most PCAs are fabricated on a semi-insulating GaAs substrate (SI-GaAs) or LT-GaAs grown on SI-GaAs. The characteristics of photoconductive materials; LT-GaAs and SI-GaAs are given in the table 2.1 below [12].

Table 2.1: Characteristics of photoconductive materials [1]

Photoconductive materials	Carrier Lifetime (ps)	Mobility (cm ² /(V.s))	Resistivity (Ω.cm)	Band Gap (eV at R.T.)
LT-GaAs	0.3	150-200	10 ⁶	1.43
SI-GaAs	50-100	1000	10 ⁷	1.43

As a result of THz emission from the semiconductor, the material properties which are represented by μ , ϵ and σ can change rapidly on a femtosecond time scale. In this time-dependent process, the biggest optically induced change is observed in the conductivity, σ [12].

In the first step for the generation, an AC bias is applied to coplanar transmission lines that are mounted on the semiconductor substrate in order to generate an electric field (in order to obtain more phase-sensitive measurements from the lock-in amplifier, AC bias is applied to the antenna). Transmission lines are used in order to transmit the energy from one point to another. This energy transfer occurs with very little energy loss. When there is no light coming to the antenna, it behaves like a capacitor with a stored energy of $E = (1/2)CV^2$ where C is the capacitance and V is the applied bias voltage. With the applied femtosecond laser pulse, the photoconductive gap is excited and the first step towards the generation of THz radiation process is launched. After that, the photons are absorbed and free electrons or holes are generated in the conduction or valence band. These electron-hole pairs created by the optical pulse are then accelerated under the applied bias voltage and decay with a time constant which is determined by the carrier lifetime of the semiconductor. The acceleration and decay of the photo-excited pairs under the applied electric field create a transient photocurrent. The current can be written as $J(t) = \sigma(t)E$ where $J(t)$ is the current, E is the electric field and σ is the conductivity affected by the carriers. More explicitly, current is $J(t) = N(t)qv(t)$ where $N(t)$ is the total carrier density, q is the electrical charge and $v(t)$ is the velocity of the carrier. Furthermore, an opposite electric field occurs in the

photoconductive gap with the separation of the electron-hole pairs and an induced polarization is created which can be described by $P(t) = N(t)qr(t)$ where $P(t)$ is the polarization and $r(t)$ is the distance between the charges at a time t . These processes occur in the subpicosecond time scale or less and this photocurrent emits the THz pulse. The electric field of the radiated THz pulse at a distance r and time t is directly proportional to the time derivative of the transient current and can be written as [47],

$$E_{THz}(r, t) = \frac{l_e}{4\pi\epsilon c^2 r} \frac{\partial J(t)}{\partial t} \sin \theta \propto \frac{\partial J(t)}{\partial t} \quad (2.11)$$

where, l_e is the effective length of the dipole, ϵ is the dielectric constant of the medium (regarded as ϵ_0 in the vacuum), c is the velocity of light in the vacuum, $J(t)$ is the current of the dipole at a time t and θ is the angle from the direction of the dipole. From the equation 2.11, it can be regarded that longer antennas have large signal amplitudes.

Furthermore, in order to collimate the THz beam, a hemispherical Si lens which has a high resistivity is attached to the PC antenna. Generally, Si material is used for the lens since it has a uniform refraction index and a very low absorption. The emitter is glued to the focus of the substrate lens in order to minimize losses due to internal reflection. Therefore, this type of substrate-lens design provides a beam without spherical aberration or coma [15, 16].

In addition, the pulsed photocurrent amplitude is dependent on the applied bias voltage and the pump laser intensity and increases linearly. Then, the radiation power also increases with the applied bias and pump power.

Generation process with photoconductive switching is a resonant interaction. The resonant frequency of a dipole antenna can be approximately written as [12]

$$\nu_r = \frac{c}{\lambda_r} = \frac{c}{2l_e\epsilon_e^{1/2}} = \frac{c}{2l_e[(1+\epsilon_d)/2]^{1/2}} \quad (2.12)$$

where λ_r is the resonance wavelength, c is the speed of light, l_e is the effective length of the dipole and ϵ_e and ϵ_d are the effective dielectric constant and the

dielectric constant of the substrate. In this equation, $\epsilon_e^{1/2}$ is equal to $(1 + \epsilon_d)/2$. Since, the generation process occurs in the substrate of the photoconductive antenna within the air, the effective dielectric constant, ϵ_e becomes the average of the dielectric constant of air which is 1 and the dielectric constant of the substrate.

In addition to the dipole antenna structure, there are several structures of photoconductive antennas such as, bow-tie antenna, and simple coplanar stripline structure [12, 17]. Emission properties, radiation spectrum and power characteristics change among these antennas as well as different substrate materials.

2.2.2. Generation of THz Radiation by Using Electro-Optic Crystal

Optical rectification is the creation of pulsed radiation in the THz range as a result of the interaction of a nonlinear EO crystal with electric field of an ultrashort pulse. Nonlinear technique that is used in the generation method by PCA is resonant but this technique is a non-resonant process where there is no photon absorption.

First of all, the theory of optical rectification and the Pockel's effect begins with an equation which polarization is proportional to the electric field of the material [1, 47].

$$P = \chi(E)E \quad (2.13)$$

where P is the electric polarization of a material, $\chi(E)$ is the electric susceptibility and E is the applied electric field. The electric susceptibility $\chi(E)$ can be complex or vector, but in optics it is generally used as a vector quantity. Therefore, the electric polarization P and the applied electric field E can be both complex and vector quantity. Moreover, by expanding the electric susceptibility $\chi(E)$ in powers of electric field E , the nonlinear properties of a material can be observed.

$$P = (\chi^{(1)} + \chi^{(2)}E + \chi^{(3)}E^2 + \chi^{(4)}E^3 + \dots)E \quad (2.14)$$

Optical rectification is a second order nonlinear optical effect and from the expansion of the electric susceptibility, it refers to the $P^{(2)} = \chi^{(2)}E^2$ term.

Three conditions should be satisfied in order to provide the optical rectification. At first, phase matching condition which means phase velocity of the THz pulse and the group velocity of the laser pulse has to be equal. Second, material of the crystal used must be transparent to both the THz and optical frequencies [11, 12, 37]. Third, the second order non-linear susceptibility has to be large at the pump wavelength.

An ideal case for the generation of THz is that the optical group velocity is equal to the THz phase velocity. Then, the velocity matching condition is satisfied and the THz field is amplified in the medium. In most cases, velocity matching is hard to achieve. If the velocities of the optical and THz pulse are different from each other, that is if the optical pulse is faster than THz pulse, the optical wave leads the THz pulse after a distance called walk-off length and is represented by [1, 47]

$$l_w = \frac{c\tau_p}{(n_T - n_O)} \quad (2.15)$$

where τ_p is the optical pulse duration, c is the speed of light in vacuum and n_T and n_O is the refractive indices of THz and optical pulses, respectively. For an appropriate condition of THz generation, the length of the nonlinear medium should have a shorter thickness than this length.

Although there are different materials used for THz generation, the most widely-used material is ZnTe crystal. The reason for using ZnTe crystal for the generation of THz pulse is that the group refractive index of the crystal is compatible with the THz refractive index at the optical wavelength of 800 nm [11]. Other optical wavelengths for which velocity matching is achieved in different crystals are listed below in the table 2.2 [10].

Table 2.2: Optical wavelengths for velocity-matching in zinc blende crystals

Crystals	ZnTe	CdTe	GaP	InP	GaAs
Wavelength (μm)	0.8	0.97	1.0	1.22	1.35

The thickness of the crystal is important in terms of strength of THz radiation and THz detection as well as the bandwidth of the generation and detection crystals. The strength of THz generation and detection is inversely proportional to the bandwidth. As the crystal becomes thinner, the strength of the radiation decreases and the bandwidth increases [15].

When the optical rectification method is compared to the photoconductive switching method it has both advantages and disadvantages. Its disadvantage is that the generated signal with PCA is more powerful than the generated signal with the nonlinear crystals because of the low efficiency in conversion of the optical frequencies to THz frequencies. On the other hand, nonlinear EO crystals can provide a wide spectrum up to 51 THz whereas the PCAs provide a spectrum of few terahertz [16].

2.3. TERAHERTZ DETECTION

2.3.1. Detection of THz Radiation by Using Photoconductive Antenna

Detection of THz pulses in the photoconductive process relies on the same physical mechanism as in the generation of THz pulses. Both the design of the antenna structure and the semiconductor material that is used affect the THz detection.

In the generation process of the THz pulse, an AC bias voltage is applied to the photoconductive antenna in order to accelerate the charge carriers along the transmission lines, however, in the detection process, the acceleration of the charge carriers are provided by the generated THz pulses. Optical pulse incident on the photoconductive antenna excites the carriers from valence band to conduction band and creates electron-hole pairs on the substrate and these carriers are accelerated by the THz pulse creating a current. Then, the current is measured on the antenna and THz pulse is examined.

2.3.2. Detection of THz Radiation by Using Electro-Optic Crystal

Electro-optic detection is the most popular choice for THz detection since electro-optic crystals are commercially available and can be found easily unlike photoconductive antennas which require micro fabrication techniques to produce them. Moreover, signals with large bandwidth can be obtained with the electro-optic detection.

For electro-optic detection, crystals such as GaSe, LiTaO₃, GaP, ZnSe and ZnTe are commonly used. Since ZnTe is very effective in THz detection and its refractive index in the far IR is comparable to the near IR, this crystal is very suitable for THz detection.

Detection of a THz-pulse beam with electro-optic crystals relies on the linear electro-optic effect which can be thought as the inverse process of optical rectification. Optical rectification states that when intense laser beam propagates through the crystal, low frequency polarization is developed. On the other hand, as the electric field is applied to the electro-optic crystal, a change in the polarization of the crystal is occurred which is known as “linear electro-optic effect” (Pockel’s effect). For both generation and detection of THz pulses, these processes are nonlinear optical techniques and occur only in crystals which are transparent to THz and optical pulses [17].

THz radiation which propagates freely can be detected by measuring the phase modulation of a laser pulse propagating through the electro-optic crystal synchronously with the THz pulse. In other words, THz pulse incident to the electro-optic crystal changes the refractive index ellipsoid of the crystal resulting birefringence which is proportional to the applied field (Pockel's effect). This causes a phase retardation of the linearly polarized optical beam and thus, the amplitude of the THz beam is measured.

$$\Delta\Gamma = \frac{2\pi}{\lambda} n^3 r_{41} l E_{THz} \quad (2.17)$$

where $\Delta\Gamma$ is the phase retardation difference, λ is the wavelength of the optical pulse, n is the refractive index of the crystal, r_{41} is the electro-optic coefficient, l is the length of the crystal and E_{THz} is the electric field of the THz radiation.

For the detection process, optical pulse and THz pulse are carefully aligned so that they should co-propagate that is they should propagate along the same direction. When linearly polarized optical beam passes through the electro-optic crystal with the THz beam, the electric field of the THz beam induces the change in the index of refraction and this change leads to a rotation of the electric field of the optical pulse by an angle which is proportional to the applied field [2, 3].

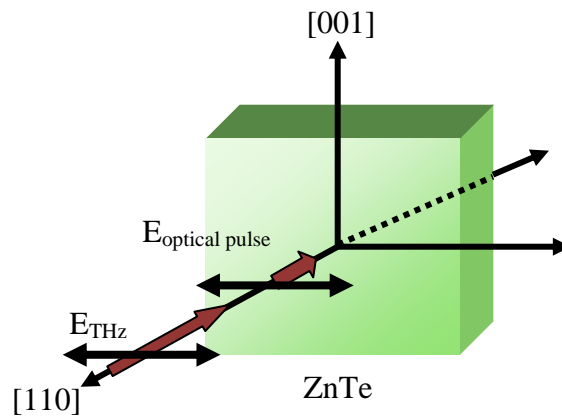


Figure 2.3: The directions of the optical and THz pulses for EO sampling [1]

As shown in the figure 2.3, the maximum induced field birefringence is occurred as the THz electric field and the optical polarization is parallel to the [110] ZnTe crystal.

The slight velocity-matching is tolerated over a distance which is denoted by [1]

$$l_c = \frac{c}{2\nu_{THz} |n_{gr} - n_T|} \quad (2.16)$$

Where ν_{THz} is the THz frequency, n_{gr} and n_T are the optical group refractive index and THz refractive index. The distance of the propagation of the optical pulse before leading or lagging the THz pulse by a phase shift of $\pi/2$ is called the coherence length.

2.4. THz TIME DOMAIN REFLECTION SPECTROSCOPY (THz-TDRS)

The methods that were used in generating and detecting THz radiation is mentioned particularly in previous sections. In this thesis, we use a photoconductive antenna for generation and an electro-optic crystal for detection of THz radiation. In the system, a mode-locked Erbium doped fiber laser is used to drive the PC antenna. The illustration of the experimental setup is shown in the figure 2.4.

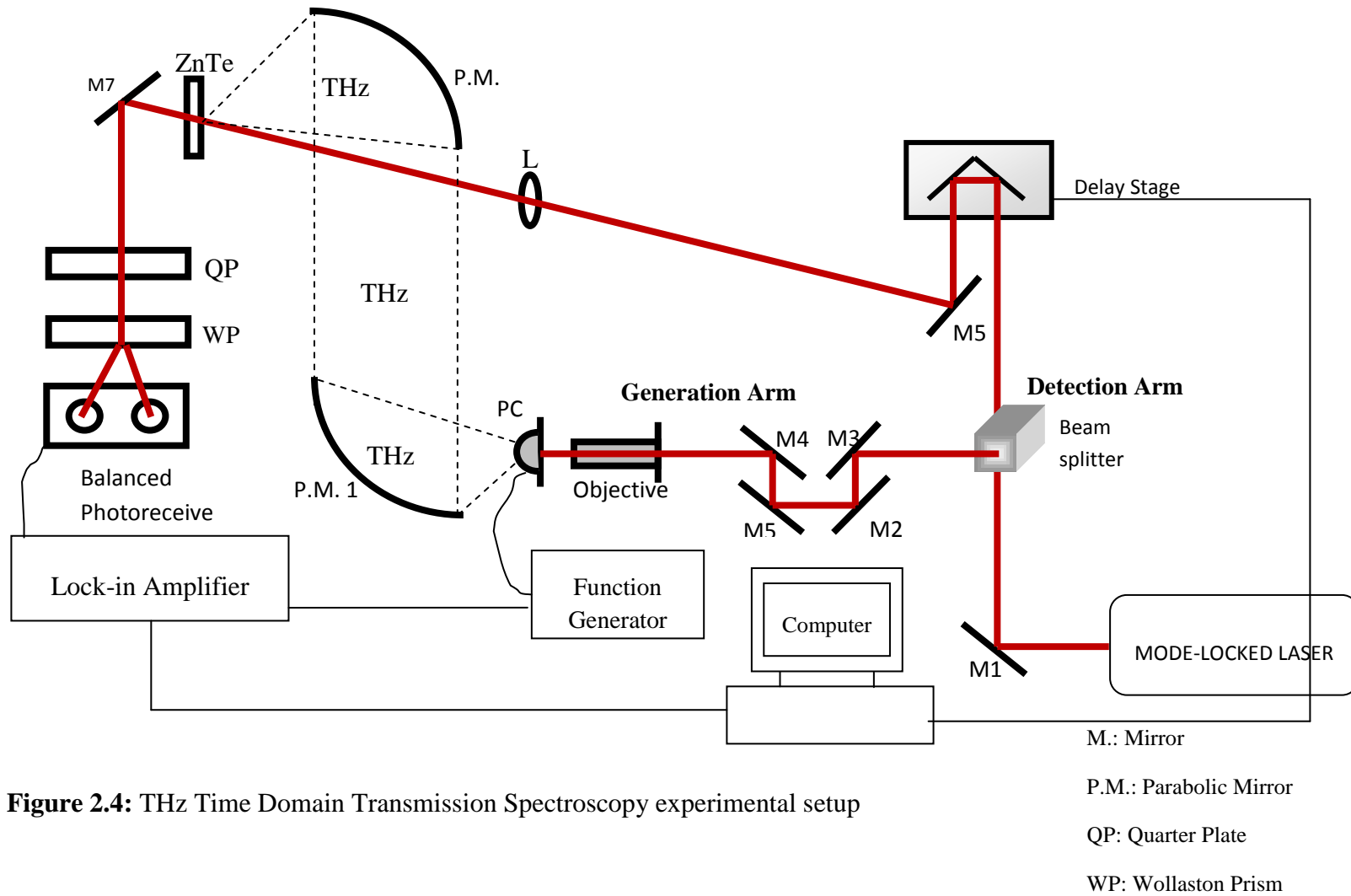


Figure 2.4: THz Time Domain Transmission Spectroscopy experimental setup

The most common method for the operation of the THz-TDS system is to separate the optical beam from a femtosecond laser into two arms. The optical pulse is divided by a beam splitter in the figure 2.4 as generation arm and detection arm in other words, pump and probe beams. In generation arm, pump pulse incident to the objective is focused onto the PC antenna and as a result, THz wave is generated. Then, parabolic mirrors as shown in the figure 2.4 as P.M.1 and P.M.2 collimate the THz radiation onto the ZnTe crystal. In detection arm, probe beam that passes through the corner cube mounted to the delay stage is focused onto the ZnTe crystal. In the system, probe beam does not propagate collinearly with THz beam. Then, this causes a decrease in the amplitude in the THz peak. Afterwards, probe beam is directed to a quarter wave plate and a Wollaston prism. A balanced photodetector is placed after these components to measure the signal and in the last step, the photodetector is connected to a lock-in amplifier and THz waveform is mapped out by a computer program.

2.4.1. System Design and Optical Components

In this thesis works, a Toptica FFS-SHG (Second Harmonic Generation) Ultrafast mode-locked Erbium doped fiber laser system with some specifications listed in the table below is employed for the both generation and detection processes. The laser power is extracted from the oscillator by an amplifier. The laser has a center frequency at 1550 nm and is frequency doubled with a PPLN crystal to 775 nm. The frequency-doubling crystal is heated to the set temperature 70°C with temperature controller.

Table 2.3: Specifications of ultrafast mode-locked Erbium doped fiber laser [18]

Peak Wavelength	~775 nm
Pulse Duration	< 150 fs
Repetition Rate	89 MHz
Average Output Power	> 60 mW

An additional optical path is created by placing 4 mirrors (M2, M3, M4, M5 in figure 2.4) in order to obtain equal paths of the generation and the detection arm. The optical pulse passing through the mirrors is directed to the 20x objective. Then, the objective focuses the optical beam to the gap of the photoconductive antenna which is mounted on the xyz translational stage. Therefore, the minimum resistance of the antenna can be obtained by moving it in three dimensions as the optical pulse is focused onto the gap. In this setup, Batop Optoelectronics PCA-44-06-10-800-x dipole photoconductive antenna with 44 μm length, 6 μm gap and 10 μm width operating at a wavelength 800 nm is used [39]. Photographic view of the antenna is given in the figure 2.5. The pump pulse should be perfectly focused on the PC antenna to get the optimum performance. Some optical and electrical properties of the antenna are given in the tables below, respectively.

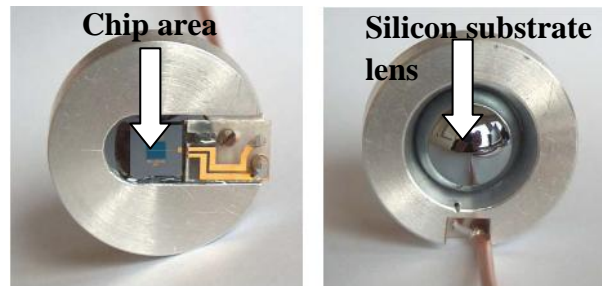


Figure 2.5: View of the photoconductive antenna in two different aspects [19]

Table 2.4: Electrical parameters of photoconductive antenna [39]

	Minimum Ratings	Standard	Maximum Ratings
Dark Resistance	20 M Ω	25 M Ω	30 M Ω
Dark Current at 10 V	300 nA	400 nA	500 nA
Voltage		20 V	50 V

Table 2.5: Optical Parameters of photoconductive antenna [39]

	Minimum Ratings	Standard	Maximum Ratings
Excitation Laser Wavelength	500 nm	800 nm	850 nm
Optical Reflectance	7 % at 500 nm	5 % at 800 nm	7 % at 850 nm
Optical Mean Power		40 mW	200 mW
Optical Mean Power Density		100 kW/cm ²	500 kW/cm ²
Carrier Recovery Time		400 fs	

In the generation process, an AC bias voltage is applied with a function generator shown in the figure 2.4. In the system, Agilent Technologies LXI-33220A Function generator was used. The frequency was adjusted to 2.5 kHz and 10V peak to peak square wave was given to the PC antenna. Applied bias voltage accelerates the free carriers along the transmission lines mounted on the photoconductive antenna and THz radiation is generated. Afterwards, the divergent THz radiation is collimated with the help of the first off-axis paraboloidal mirror (P.M.1 in figure 2.4) and focused onto the <110> oriented ZnTe detection crystal whose thickness is 1 mm by the second off-axis paraboloidal mirror (P.M.2 is figure 2.4). These off-axis paraboloidal mirrors are produced by CVI Melles Griot have a focal length 119.4 mm [40].

In the detection process, the probe beam is passed through the corner cube mounted on a translation delay stage in order to satisfy the velocity match of the optical and THz pulse and finally, the beam is focused onto the detection crystal by a lens of 20

cm focal length (L1 in the figure 2.4). As the optical pulse and the THz radiation overlap in the electro-optic crystal, the electric field of the THz pulse changes the refractive index and the polarization of the probe beam is changed.

After the electro-optic detection crystal, a quarter wave plate and a Wollaston prism is placed and the induced probe beam is directed to these components by a mirror (M7 in figure 2.4). A quarter wave plate was used to convert linearly polarized light into circularly light. Next, as the pulse passes through the Wollaston prism, it is separated into two orthogonal linearly polarized light beams. The configuration of electro-optic crystal, a quarter wave plate and a Wollaston prism is seen in figure 2.6. The polarization difference is measured by placing these components respectively.

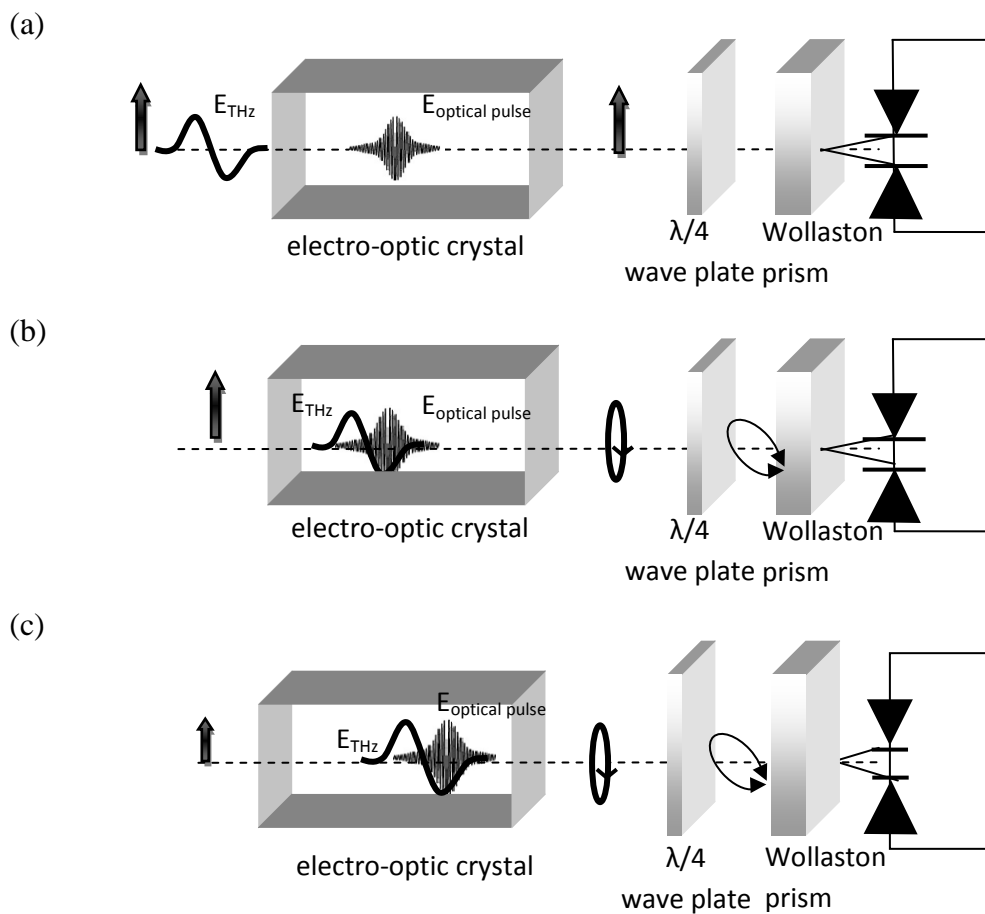


Figure 2.6. EO sampling

As shown in figure 2.6 (a), after the crystal, when there is no THz, as the optical beam passes through the quarter wave plate, linearly polarized light is converted into circularly polarized light. Wollaston prism after the quarter wave plate splits the circularly polarized light into two components which are orthogonal and linearly polarized to each other and each component is detected by a balanced photo-receiver. The components of the polarized light become equal when THz is not present. In other words, without THz beam, two modes of the propagating light will be subjected to the same phase retardation.

In figure 2.6 (b), electric field of the optical pulse coincides with the negative electric field of the THz radiation by delaying the optical pulse. Then, an induced birefringence is occurred and the polarization of the optical pulse changes due to this birefringence. Moreover, due to this birefringence, the components of the optical beam propagating through the crystal are subjected to different phase retardations.

After the overlapping of the optical pulse and the THz radiation through the crystal, the optical polarization at the exit of the electro-optic crystal has been slightly rotated like elliptically relative to the entrance of the crystal after the quarter wave plate. Then, elliptically polarized light is separated into two linearly and orthogonal beam by the Wollaston prism and finally the intensities of these two components are detected by the balanced photo.

In figure 2.6 (c), in this case, the electric field of the optical pulse and the positive electric field of the THz radiation overlap in the electro-optic crystal by changing again the delay of the optical pulse. Again, birefringence occurs and the polarization of the optical pulse is changed in the opposite direction relative to the previous case in which the negative electric field of the THz radiation and the optical pulse coincides. Therefore, the opposite rotation of the polarization of the optical pulse is detected by the balanced photodiode in terms of difference in intensities of the two components.

The difference of the intensities of the components of the pulse is detected by a New Focus 2307 Large Area Balanced Photoreceiver connected to a lock-in amplifier as shown in the figure 2.4. In this spectrometer, a Stanford Research Systems SR830

Model lock-in amplifier was used [41]. Basically, lock-in amplifiers which are phase-sensitive detectors can measure very small signals that vary on the order of nanovolts. The basic operating principle of the lock in amplifiers is to choose one component of the signal (in phase or 90 degree out of phase component) at a specific reference frequency and reference phase. A reference frequency is required to detect the response of the probe pulse according to the modulated THz beam at that reference frequency. Therefore, both the amplitude and the phase of the signal can be obtained [20].

To map out the entire waveform, the delay time of the optical and THz pulse can be adjusted by the linear motion of a translational stage controlled by a Thorlabs APT Stepper Motor Controller BSC103 (as shown in figure 2.4) which is controlled by a program written in Lab View code [38]. With the help of this program, both the Time and Frequency Domain spectra can be obtained. The step size of the translational stage, wait time durations and the position intervals can be adjusted by using the program.

An example of a measurement that is taken with the set-up shown in the figure 2.4 as the pulse propagating through the free space is shown in the graph below.

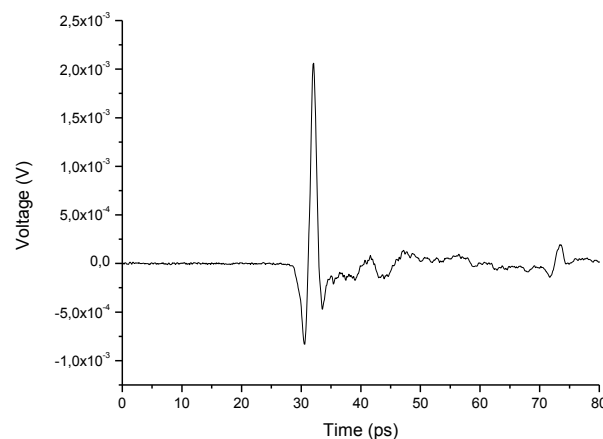


Figure 2.7: THz waveform before placing the reflectance mirrors and TPX lenses

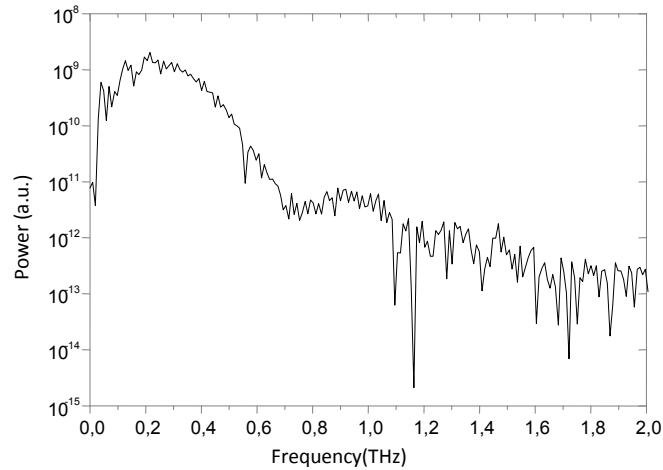


Figure 2.8: Power spectrum of the THz waveform before placing the reflectance mirrors and TPX lenses

In the case of samples that are opaque in the THz frequency range, the transmission geometry in THz-TDS is not appropriate. Therefore, THz-TDRS is required. In THz-TDRS systems, a reference measurement which can be done off of a mirror with a high reflectivity is required as compared to transmission spectroscopy [21].

In the experimental setup, the main property that differs from transmission spectroscopy is that the reflection mirrors are placed near the paraboloidal reflectors and TPX lenses are used to focus onto the reference mirror as shown in the figure 2.9.

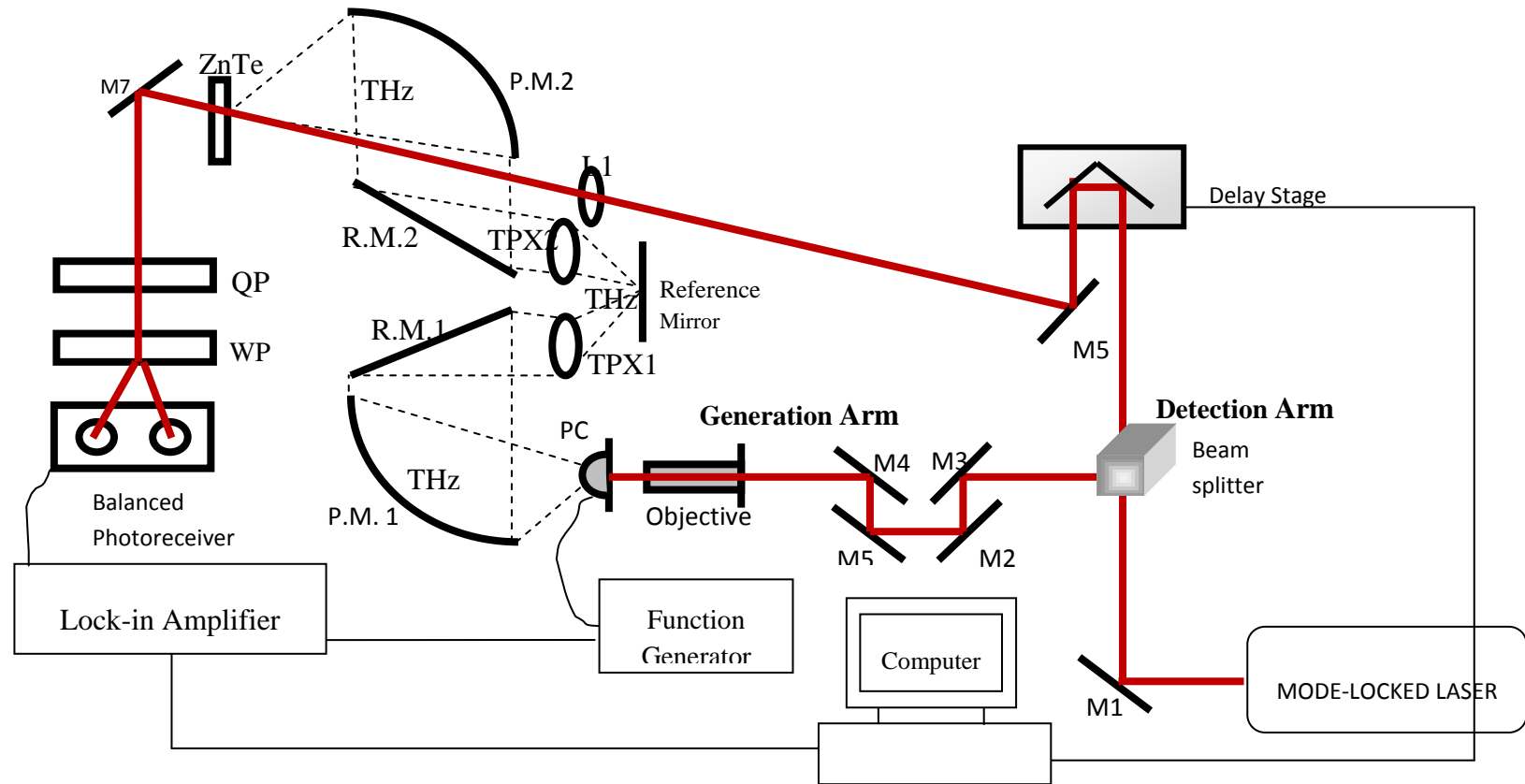


Figure 2.9: THz-TDRS experimental setup with paraboloidal reflectors and TPX lenses

The collimated beam reflected from the first reflection mirror (R.M.1 in the figure 2.9) is focused by a TPX lens (TPX1 in the figure 2.9) with focal length of 15 cm and a diameter 5 cm onto the reference mirror in the figure 2.9. Next, the reflected beam from the reference mirror is collimated by another TPX lens (TPX2 in the figure 2.9) with the same properties as the focusing mirror and directed to the second paraboloidal mirror. After that, THz radiation is focused onto the electro-optic crystal by the paraboloidal mirror.

Reflection mirrors used in the spectrometer are gold-coated in order to prevent the amplitude loss in the signal. The lenses that were used to focus the THz radiation onto the reference mirror are made up of TPX material. TPX lenses have lower absorption and the average refractive index is lower than the polystyrene and polymers that is the transmission loss is lower. Moreover, TPX is the lightest among the other polymers, it is transparent to visible and THz [41].

Example of a reflectance measurement that is taken with the set-up shown in figure 2.9 after placing the mirrors and TPX lenses is shown in the graph below.

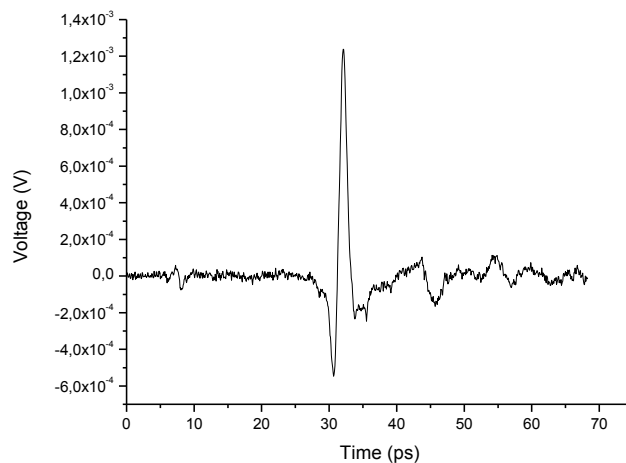


Figure 2.10: THz waveform after placing the reflectance mirrors and TPX lenses

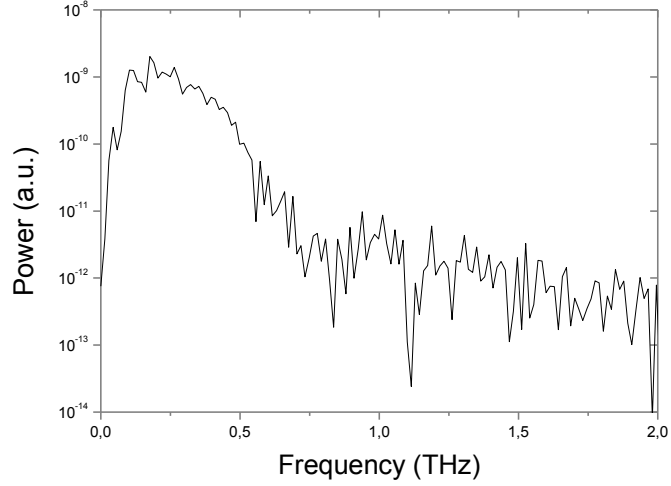


Figure 2.11: Power spectrum of the THz waveform after placing the reflectance mirrors and TPX lenses.

According to the THz time-domain graph as shown in figure 2.10 the signal to noise ratio is approximately 100:1.

The beam parameters of the focused THz beam in order to calculate the spot size of the beam are given in the equations below, respectively.

$$\theta = \frac{1.22\lambda}{d_{in}} \quad (2.18)$$

Where θ is the angular divergence of the beam, λ is the wavelength and d_{in} is the entrance diameter.

$$d_{out} = f\theta \quad (2.19)$$

Where d_{out} is the exit diameter, f is the focal length of the lens.

$$\omega_0 = \left(\frac{\lambda z_0}{\pi}\right)^{1/2} \quad (2.20)$$

Where ω_0 is the beam waist, z_0 is the Rayleigh range.

$$\omega(z) = \omega_0 \left[1 + \left(\frac{z}{z_0}\right)^2\right]^{1/2} \quad (2.21)$$

Where $w(z)$ is the width of the beam and z is the axial distance from the beam's narrowest point.

The parameters of TPX lenses are: entrance diameter d_{in} is 50 mm, focal length, f , of the lens is 150 mm. The peak frequency from the power spectrum in figure 2.11 is 0.18 THz.

Then, with the given parameters and equations, THz is focused on a spot size of 6 mm.

2.5. MEASUREMENTS ON THE SILICON WAFER

THz-TDS is a powerful tool in measuring the samples at THz frequencies. The measurements are based on the change in the electric field through both a sample and reference (air). Terahertz time domain spectroscopy means the measurements are obtained by the changes in temporal shape of the electric field strength of the THz pulse.

Two types of measurements should be made: with and without sample. For the pulse that propagates through the sample or reflected off of the sample, the pulse is called a sample pulse; if the pulse propagates through air, the pulse is called reference pulse. In this section, sample and reference measurements are given for a silicon wafer in reflection mode.

In time domain THz spectroscopy, the measurements are obtained in time domain. By applying Fourier transform to the both measurements, spectral components as well as phase information are obtained. In the figure 2.10-11, the reference and the sample pulse measurements are given.

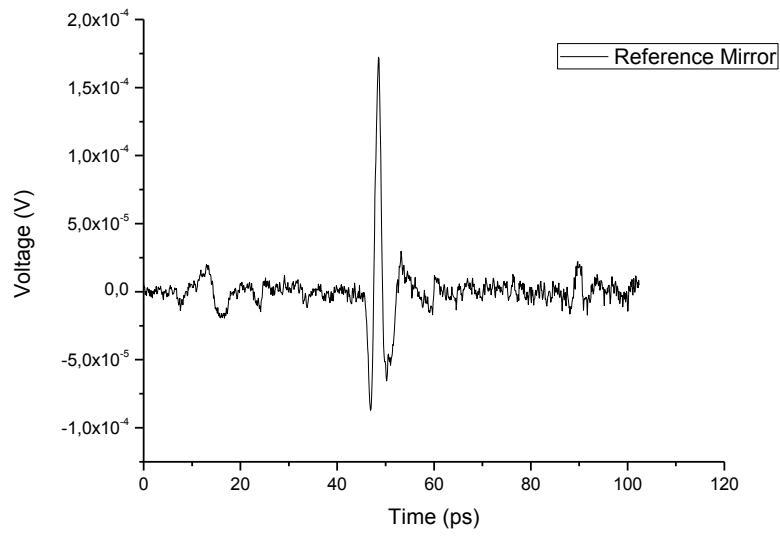


Figure 2.12: THz waveform of reference mirror

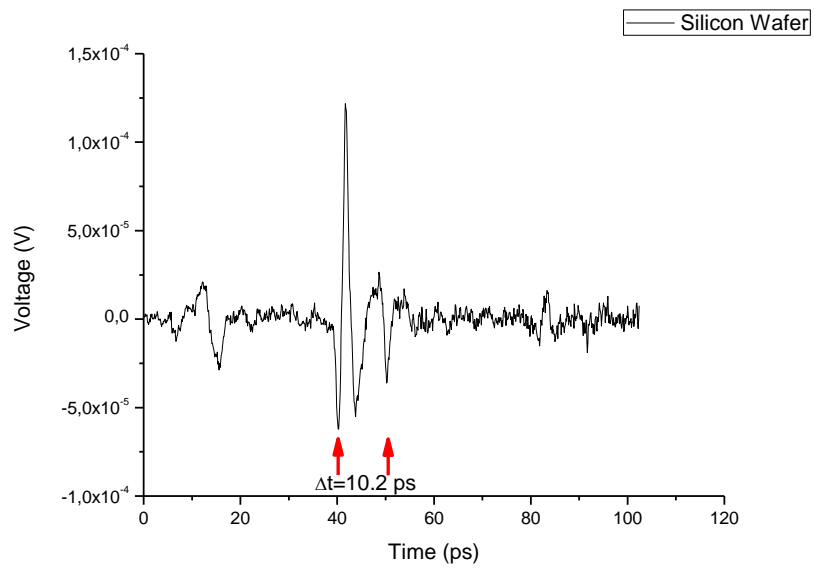


Figure 2.13: THz waveform of the silicon wafer

As mentioned before, refractive index of a sample can be calculated from the equation 2.8, however, in our case refractive index cannot be calculated as given by this formula since there is no phase difference. Therefore, the refractive index of the silicon wafer can be calculated from

$$n = \frac{c\Delta t}{2l} \quad (2.18)$$

where c is the speed of light 3×10^8 m/s, Δt is 10.2 ps from the figure above between the peaks and l is 0.45 mm which is the silicon wafer thickness. Therefore, with these parameters, the refractive index of the silicon wafer can be calculated as 3.4.

Moreover, since silicon is used in solar cell technologies, before we measure the THz reflection off solar cells we wanted to see if the THz reflection amplitude would change when an un-doped silicon wafer is illuminated with visible light. The wavelength of illumination was chosen to be 808 nm since this was the most powerful source of continuous single frequency radiation we had in our laboratory. This laser emitted a power of greater than 500mW. 808nm is a useful illumination for silicon as can be seen from its response curve in figure 2.14.

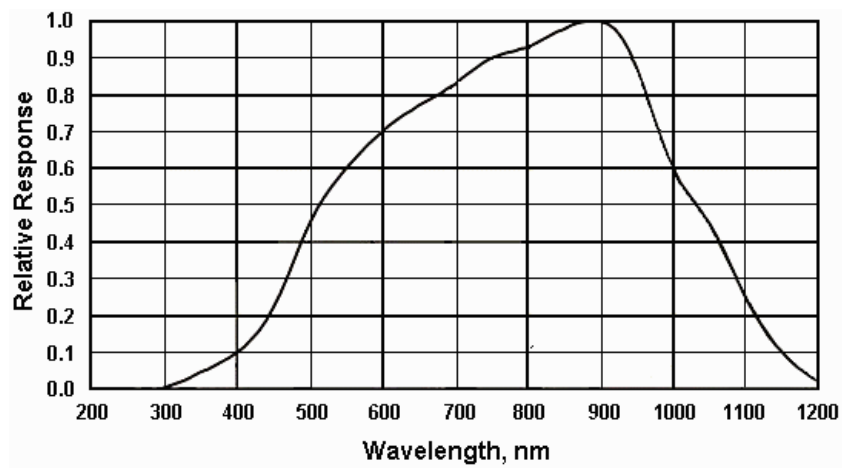


Figure 2.14: Spectral response curve of silicon [36]

The experimental setup of the THz measurements were done with and without applying 808 nm Diode Laser to the sample and the figure of these obtained THz waveforms is shown below.

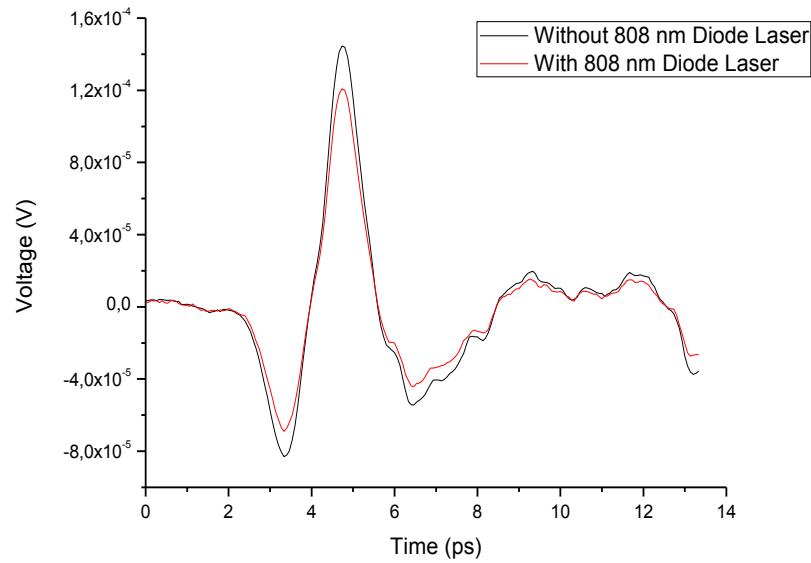


Figure 2.15: Comparison between the THz waveforms in both measurements

As can be seen from the figure 2.15 above, there is a difference in the amplitudes of the THz pulses with and without illumination. The THz pulse under illumination with 808 nm Diode Laser is lower than the THz pulse with no illumination with the same laser. This change in the reflection amplitude is a useful indication that we can use THz-TDS to measure electrical properties of silicon solar cells under optical illumination.

CHAPTER 3

OPERATION PRINCIPLES OF SOLAR CELL

Traditional sources of energy like coal, fuel and oil are running out faster day by day. Due to increasing energy demands for the future, photovoltaic conversion of solar energy has gained much importance today.

Photovoltaic devices are the most environment-friendly sources that generate electricity. It is an alternative method to conventional fossil fuel electricity generation. The first practical photovoltaic device was produced in the 1950s so it is a newcomer and is a rapidly growing technique compared to other electricity generation methods [26]. Moreover, a photovoltaic cell must be effective in that it should have a long operation lifetime to overcome its financial impact mainly being the high energy cost for the initial production. Spectrum of the incident light, radiant power density from the sun, the angle of the incident solar radiation that strikes the photovoltaic device, the radiant energy from the sun throughout a year or a day for a particular surface are some of the important properties of the incident solar energy that affect the interaction between the incident sunlight and a photovoltaic device or any other object [33].

In this chapter, first brief information about the properties of sunlight is given. Second, some properties of semiconductors that is used in the production and operation of solar cells is discussed. Since typically silicon crystals are used in the design of solar cells, silicon crystal properties will be especially discussed in this chapter. Then, the structure and the operation principle of a solar cell will be explained.

3.1. SEMICONDUCTOR MATERIAL PROPERTIES

3.1.1. Structure of Semiconductors

Semiconductors are the materials which have resistivity in the range of 10^{-2} - 10^9 cm. Based on the purity these materials can be grouped as intrinsic or extrinsic. The other classification for the semiconductors is being n-type or p-type, depending on their majority carriers either electrons or holes. Moreover, due to their structure properties, they can also be single crystal, amorphous or polycrystalline. By doping process, impurity atoms can be added to a semiconductor in order to change the charge concentration which vary the conductivity and shift the balance of electron and holes in the structure. The band gap energy E_g of a semiconductor is defined as separation between the top of valance band energy (E_v) and the bottom of conduction band energy (E_c). Band diagram of the different materials (metal, insulator, and semiconductor) and the energy transition of electrons in a semiconductor can be seen in figure 3.1 and 3.2, respectively.

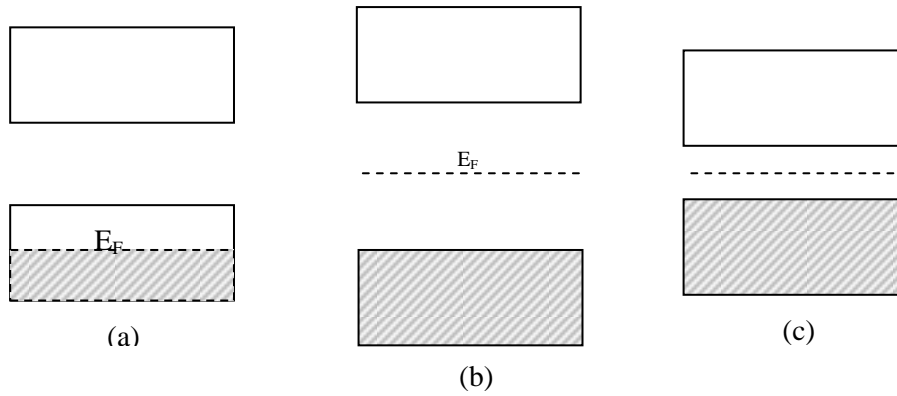


Figure 3.1: Allowed states that are occupied by electrons in (a) a metal, (b) an insulator, (c) a semiconductor. Fermi level is used to describe the top of the collection of electron energy level at absolute zero. It gives information about the probability of occupation of an electron in a given state [26].

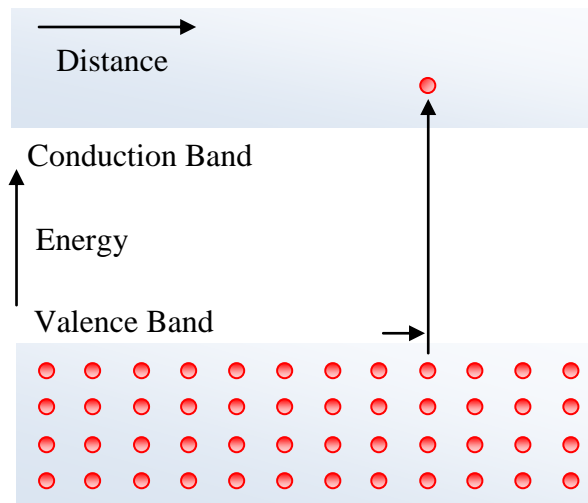


Figure 3.2: Band Diagram of a semiconductor [35]

The energy and momentum of an electron in semiconductors are related by an equation

$$E = \frac{p^2}{2m} \quad (3.3)$$

Where E is the energy, p is the momentum and m is the mass of the electron. In some semiconductors, for the electrons in the conduction band at the energies close to the minimum energy in the conduction band and for the holes in the valence band at the energies close to the maximum energy in the valence band, the relationship between the energy and momentum is written [28]

$$E - E_c = \frac{p^2}{2m_e} \quad \text{and} \quad E_v - E = \frac{p^2}{2m_h} \quad (3.4)$$

respectively. Where E_c is the energy in the conduction band, E_v is the energy in the valence band, p is the momentum, m_e and m_h is the mass of the electrons and holes, respectively. With the absorption of photons, an electron excites from the valence band to the conduction band leaving a hole in the valence band. In this process, energy and momentum are conserved. A photon has a quite small momentum (h/λ) and a large energy. These semiconductors are called direct-band-gap semiconductors, and the most widely used one is GaAs.

In other semiconductors, the same relation between energy and the momentum for electrons and holes can be written as [28]

$$E - E_c = \frac{(p-p_0)^2}{2m_e} \quad \text{and} \quad E_v - E = \frac{(p-p'_0)^2}{2m_h} \quad (3.5)$$

In this case, the photon energies larger than the band gap energy gives rise to electron from the valence band to the conduction band. However, a third particle, phonon contributes to the process. A photon has a low energy but a high momentum. Then, in this condition, the transition gains momentum. These types of semiconductors are known as indirect-band-gap semiconductors and the most widely used one is Silicon.

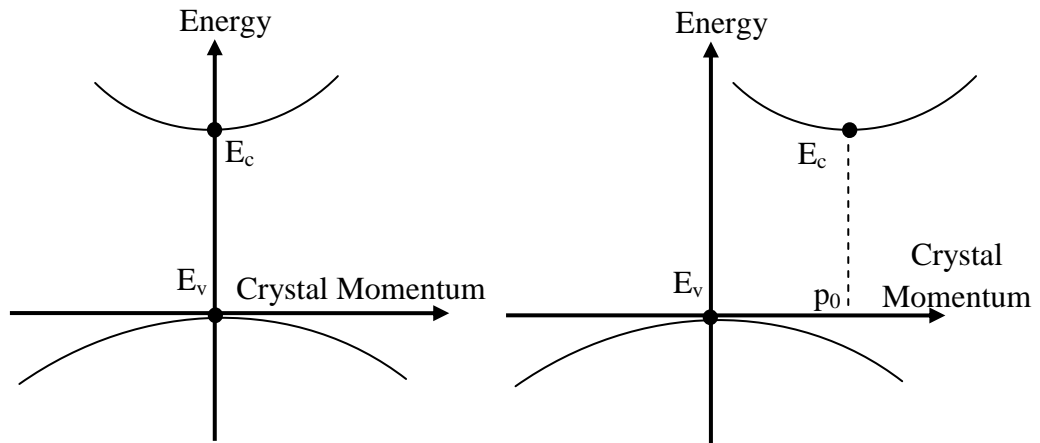


Figure 3.3: Energy-crystal momentum relations for a (a) direct-band-gap (b) indirect-band-gap semiconductor [30].

For a solar cell operation, there are some important parameters such that the band gap, the number of free carriers and the generation and recombination of free carriers due to the effect of light colliding on the material.

3.1.2. Intrinsic Carrier Concentration

With the thermal excitation, as an electron moves from the valence band to the conduction band results free carriers in the bands and the concentration of these carriers is called intrinsic carrier concentration. The number of the electrons in the conduction band or the holes in the valence band gives the intrinsic carrier concentration. The temperature and the band gap of the material affect the number of carriers. In the large band gap semiconductor, the difficulty of the excitation of an electron from the valence band to the conduction band across the band gap causes the lower intrinsic carrier concentration. Moreover, the increase in the temperature

results excitation of more electrons to the conduction band and an increase in the intrinsic carrier concentration.

The concentration of electrons and holes can be changed by doping with other types of atoms in a silicon crystal. In doped material, one type of carrier is always more than the other type of carrier and the carrier with higher concentration than the other is called the majority carrier and the other is called the minority carrier. If the doped atom has more valence electron than silicon in the valence band, the material will be n-type semiconductor material. The number of electrons will be higher compared to holes and the majority carriers will be negatively charged carriers. On the other hand, with fewer electrons in the valence band, the material will be p-type semiconductor. The number of holes will increase and the majority carriers will be positively charged holes [33, 35].

If there is no external applied bias, the number of carriers in the conduction and the valence band is the equilibrium carrier concentration. The equilibrium carrier concentration is equal to the number of free carriers plus the intrinsic carrier concentration. The product of majority and minority carrier concentration is constant at equilibrium condition and it is denoted by the Law of Mass Action [36].

$$n_o p_o = n_i^2 \quad (3.6)$$

where n_o and p_o are the equilibrium carrier concentration of electron and hole and n_i is the intrinsic carrier concentration.

3.1.3. Absorption of Light

Three processes of photons that are incident on the surface of a semiconductor are reflection, absorption and transmission. For photovoltaic devices, reflection and transmission do not contribute to the operation of the devices since photons that are not absorbed do not interact with the semiconductor, so there is no effect on the electrons. As the photon is absorbed in the material, an electron is excited from the

valence band to the conduction band. The comparison of energy of the photon with the band gap energy of the semiconductor gives the interaction of the photon with the semiconductor. If the energy of the photons is less than the band gap energy, photons do not interact and passes through the material. If the photon energy is greater than the band gap, it is strongly absorbed in the material and electron-hole pair is created. An absorbing material has an index of refraction, \hat{n}_c , a complex number. This number can be written explicitly in the form of $\hat{n}_c = \hat{n} - i\hat{k}$. Here, \hat{k} is the extinction coefficient. The fraction of light reflected form the surface at normal incidence can be written as [36]

$$R = \frac{(\hat{n} - 1)^2 + \hat{k}^2}{(\hat{n} + 1)^2 + \hat{k}^2} \quad (3.7)$$

For the appropriate values of crystal silicon, over 30% of the incident light is reflected which is an undesirable condition. In order to obtain efficient solar cells, antireflection coatings or other techniques to reduce the reflection are used in solar cells.

The penetration distance of a particular wavelength of light before its absorption is the absorption coefficient. Wavelength of light which is being absorbed and the material are important parameters in determining the absorption coefficient. If the photon energy is very close to the band gap energy of the material, the absorption will be very low because electrons which are at the edge of the valence band will interact with the photon and absorption will be occurred. When the energy of the photon is increased, the interaction of electrons with the photons increases which causes strong absorption. On the other hand, for photovoltaic devices, as the photon energy is much greater than the band gap energy, electrons thermalize back down to the edges of the band so the excess energy is wasted. The relationship between the absorption coefficient and the wavelength can be defined as

$$\alpha = \frac{4\pi k}{\lambda} \quad (3.8)$$

Where α is the absorption coefficient, k is the extinction coefficient and λ is the wavelength [33].

Different wavelengths are absorbed in different distances in the material. The absorption depth is generally defined as the inverse of the absorption coefficient, α^{-1} .

3.1.4. Generation Rate

Generation rate is related to the absorption of photons in the material and the numbers of electrons generated in the device gives the generation rate. Absorption coefficient and the thickness of the material determine the absorption process. The number of electron-hole pairs generated in a solar cell can be calculated from the intensity of light formula [31].

$$I = I_0 e^{-\alpha x} \quad (3.9)$$

where I_0 is the intensity of light on the top of the surface, α is the absorption coefficient and x is the distance in the material that the intensity of light is calculated.

As the photons in the light are absorbed, the intensity of light decreases and electron-hole pair is generated. Therefore, the change in the intensity of light through the material gives the generation G . If the derivative of the above equation is taken, the generation rate at an arbitrary point in the material is written as

$$G = \alpha N_0 e^{-\alpha x} \quad (3.10)$$

where α is the absorption coefficient, N_0 is the photon flux at the surface and x is the distance in the material that the generation rate is calculated [27]. Light consists of different wavelengths, so the generation rate is different at each different wavelength.

3.1.5. Types of Recombination Process

As the electron excites to the conduction band, it becomes unstable and move back to its initial energy state in the valence band. In this recombination process, the created hole will be removed. For the single-crystal semiconductors, radiative, Auger and Shockley-Read-Hall recombination are the three different types that play an important role. In radiative (band-to-band) recombination, an electron-hole pair is created and as a result photon is emitted as shown in the figure [27].

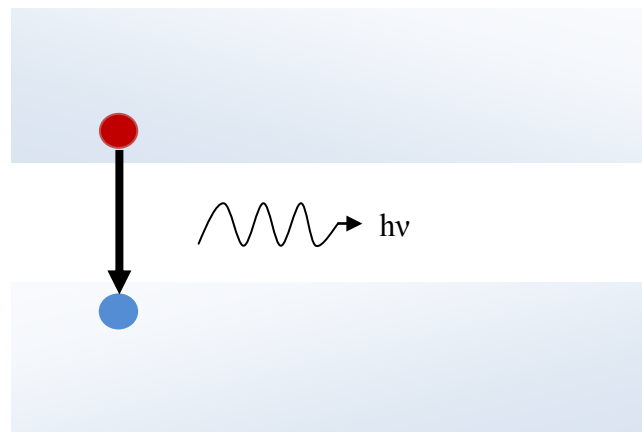


Figure 3.4: Radiative (Band-to-Band) Recombination

Moreover, radiative recombination is common in direct band gap semiconductors. However, most solar cells are made up of silicon which has an indirect band gap. Therefore, radiative recombination is very low in silicon solar cells. Shockley-Read-Hall is common in defected material due to doping. This process is occurred as the trapped electron or hole in the forbidden region is recombines with another hole or electron which moves up to the same energy state [29].

Auger recombination is dominated in heavily doped or excited material. In this type of process, there are three carriers. As the electron and the hole recombine, the emitted energy is given to a third carrier in the conduction band and the third carrier is pushed to the higher levels in the conduction band and then it moves back to the conduction band edge [32].

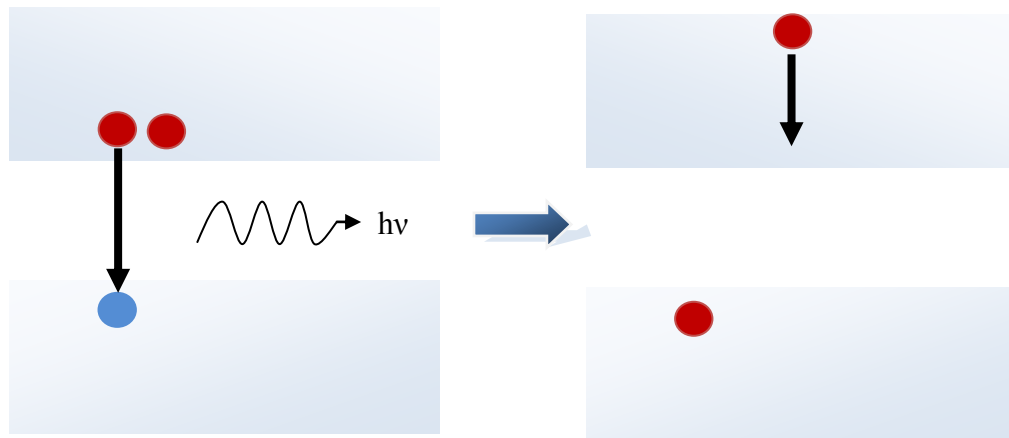


Figure 3.5: Auger Recombination [28]

3.1.6. Lifetime

The time interval that the minority carriers which are generated by incident light on the material stay stable before the recombination process is called lifetime. Solar cells with long minority carrier lifetimes are generally more efficient than the short minority carrier.

In a doped material where the minority charge carriers are less, the lifetime is written as [30]

$$\tau = \frac{\Delta n}{R} \quad (3.11)$$

where τ is the minority carrier lifetime, Δn is the excess minority carrier concentration and R is the recombination rate.

3.1.7. Diffusion

If one region has a lower concentration than the other region in the material, the carriers move from the high concentration region to the low concentration region. With the random motion carriers flow one region to another is called diffusion [31]. Diffusion rate can be determined by the speed of carriers. Therefore, if the temperature is increased, thermal velocity of the carriers increase, then the diffusion occurs faster.

Without electric field, the carriers move in a random direction with a velocity. If an electric field is existed in the material, holes move in the direction of the applied electric field with acceleration and electrons move in the opposite direction of the electric field.

3.1.8. P-N Junction

P-n junction diodes are the most basic part of the many electronic devices consisting of solar cells, lasers, and Light Emitting Diodes (LEDs). N-type and p-type semiconductors form p-n junctions. Electrons move from n-type region to p-type region and holes move in the opposite direction since n-type semiconductors have high electron concentration and p-type semiconductors have high hole concentration. Without electric field, the diffusion from one region to another continues as the concentration of the both sides become equal. If the holes and electrons move to the other region, they leave behind negative and positive ion cores, respectively. An

electric field is occurred between these ion cores in a region called depletion region. The reason why this region is called depletion region is that this area is depleted of free carriers.

If there is no electric field of external effect on the p-n junction, there is an equilibrium condition between carrier generation, recombination and diffusion.

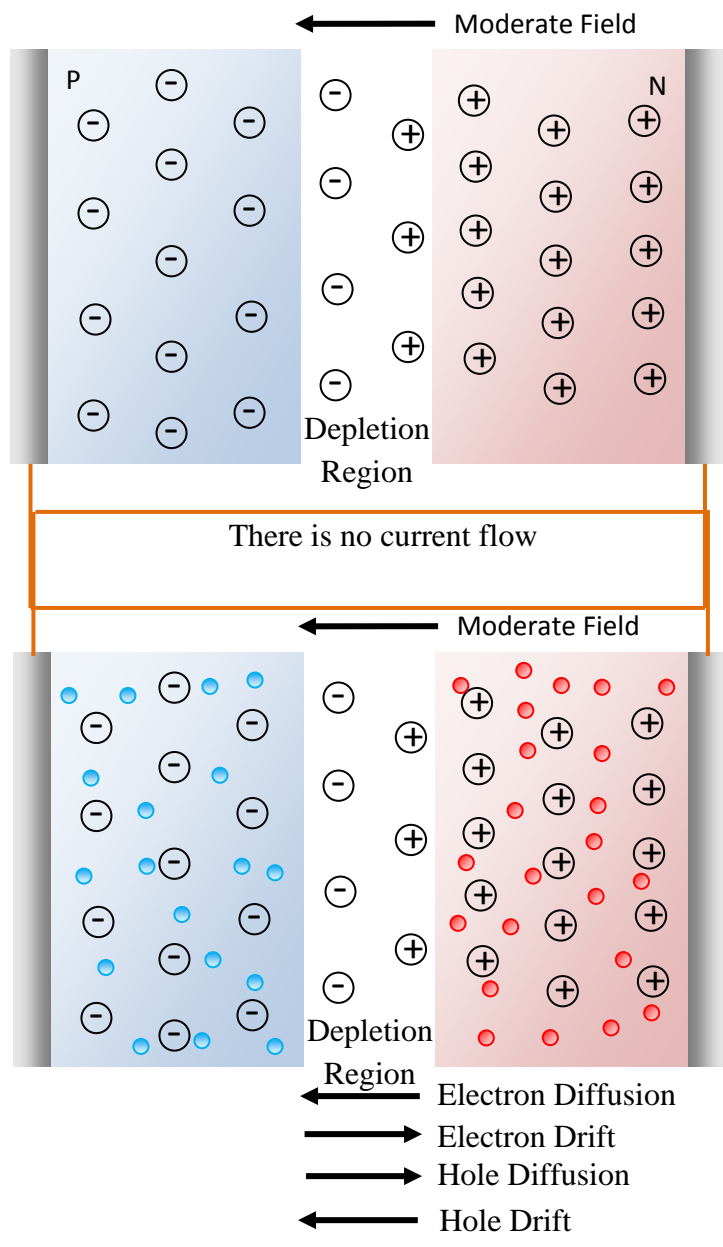


Figure 3.6: P-N junction Diode Structure [32]

The three conditions that the semiconductor devices operate are thermal equilibrium, steady state and transient. In thermal equilibrium, there is no net current in the device and the current is balanced, therefore, there is no external effect acting on the device. In steady state condition, there is no change with time despite there are external

effects such as light or applied voltage. In transient condition, due to rapid change in the applied voltage, there will be a short delay in the operation of a solar cell.

In forward bias, by applying voltage across the material the electric field is decreased. An electric field in opposite direction is created, as positive and negative voltage is applied to the p-type and n-type semiconductor, respectively.

The current flow through a diode as a function of voltage is given by the ideal diode law and can be written as [29]

$$I = I_0 \left(e^{\frac{qV}{kT}} - 1 \right) \quad (3.12)$$

where I is the net current flowing through the diode, I_0 is the dark saturation current with no light, V is the applied voltage through the diode, q is the charge of one electron, k is Boltzmann's constant and T is the temperature in K.

Each diode has a unique dark saturation current I_0 and it is a measure of the recombination. However, for actual diodes, ideality factor n is added to the equation and the new equation becomes [27]

$$I = I_0 \left(e^{\frac{qV}{nkT}} - 1 \right) \quad (3.13)$$

The ideality factor changes between 1 and 2 due to the diode characterization.

3.2. SOLAR CELL OPERATION

3.2.1. Structure of Solar Cell

A solar cell directly converts sunlight into electricity. As light strikes the solar cell, a current and a voltage is produced and so power is generated. As the light is absorbed through the material, an electron is excited to the higher state. Then, the electron in

the higher state flows from the solar cell to the external circuit and gives its energy to the circuit and returns back to the solar cell again. For this photovoltaic energy conversion, p-n junction semiconductor materials are needed. The basic structure of a solar cell is shown in the figure 3.7.

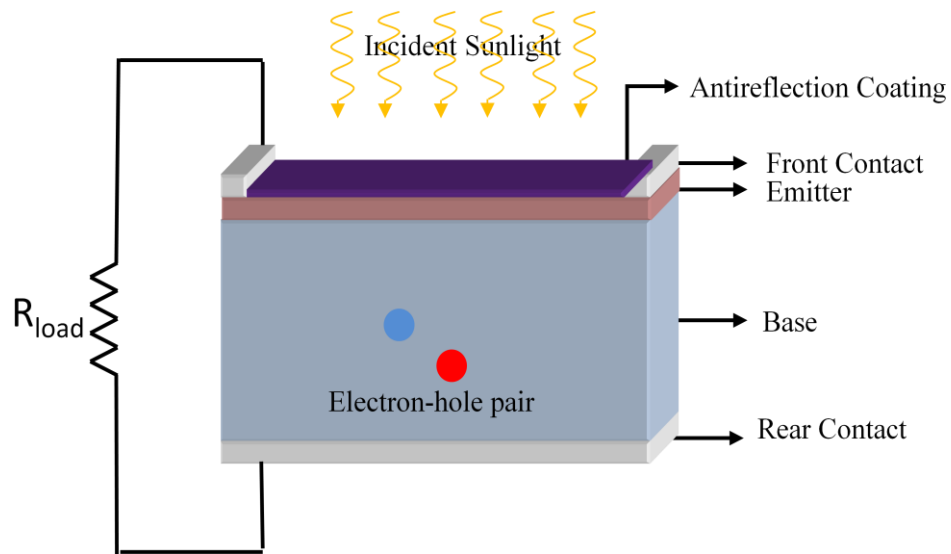


Figure 3.7: Solar Cell Structure

Current is generated in a solar cell as the incident photons are absorbed through the material in order to create electron-hole pairs. The most important condition for the generation of electron-hole pairs is that the energy of the incident photon should be equal or greater than the energy of the band gap of the semiconductor. Before the recombination process, electrons and holes are not stable during the time which is equal to the minority carrier lifetime. As the carriers recombine, the electron-hole pairs are lost and the current and voltage is not generated anymore.

P-n junction prevents recombination process by separating the electron and the hole. Carriers are separated by the electric field in the p-n junction. If the emitter and the base of the solar cell are connected with each other, the carriers of light generated flow through an external circuit.

3.2.2. Quantum Efficiency (Q.E.)

The relationship between the number of carriers collected by the solar cell and the number of photons incident on the solar cell gives quantum efficiency. If all photons of a certain wavelength are absorbed and all carriers are collected by the solar cell, then the quantum efficiency at that wavelength is unity. Recombination and collection probability affect the quantum efficiency. There are two types of quantum efficiency which are internal and external. Internal quantum efficiency of a silicon solar cell can be calculated from the incident photons that are not lost during reflection and transmission from the solar cell and generate collectable carriers [31, 32]. External quantum efficiency can be calculated from the incident photons that remain after transmission and reflection.

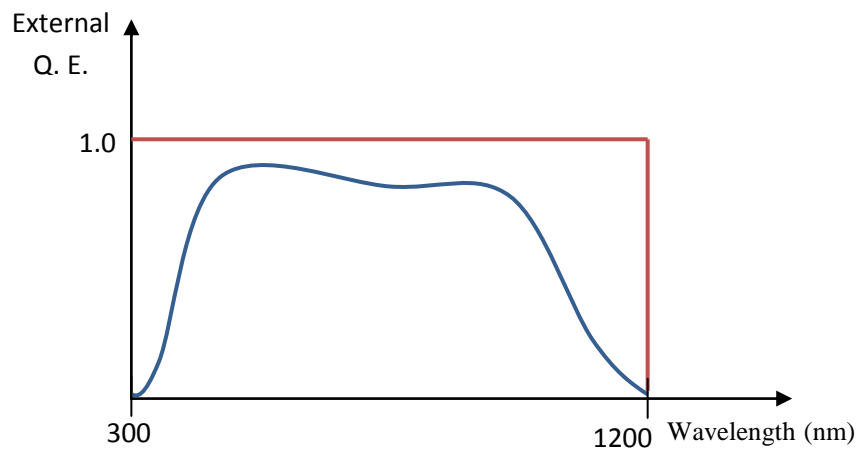


Figure 3.8: Quantum Efficiency of a silicon solar cell [32]

In the above graph, the ideal quantum efficiency is 1 which is drawn in red line and quantum efficiency is zero at long wavelengths since light is not absorbed under the band gap.

3.2.3. Spectral Response

Another parameter for a solar cell is the spectral response which is very similar to the quantum efficiency. The ratio of the current generated by the solar cell to the power of the incident light on the device gives spectral response. At long wavelengths, the energy of the photons at these wavelengths is lower than the band gap energy of the semiconductor. Therefore, the spectral response cannot be determined in this condition. Moreover, the relationship between the quantum efficiency and the spectral response can be shown as [33]

$$SR = \frac{q\lambda}{hc} QE \quad (3.14)$$

where SR is spectral response, q is the charge, λ is the wavelength of the incident light, h is the Planck's constant, c is the speed of light and Q. E. is the quantum efficiency.

3.2.4. Photovoltaic Effect

As mentioned before, in order to generate power, a current and the voltage must be generated. Photovoltaic effect is the generated voltage in the solar cell. As the light generated carriers are collected by the p-n junction, there is a movement of electrons to the n-type region and holes to the p-type region. If there is no short circuit, the carriers do not leave the device and the number of carrier increase in both sides. Then, an electric field is created between these carriers in opposite direction to the

already existing field [26]. Therefore, the net electric field in the device is decreased. A barrier is created due to electric field for the flow of forward bias diffusion current. As the net electric field decreases in the solar cell, the flow of diffusion current increases. The current flowing from the solar cell is the difference between the light generated current and the forward bias current. As the forward bias current and the light generated current is balanced, the net current flowing through the device becomes zero.

3.3. CHARACTERIZATION OF A SOLAR CELL

In this section, the parameters that are used in the efficiency calculation of a solar cell are described. By using known techniques with these parameters and known measurement methods, the efficiency of the solar cell is calculated in the next chapter and the results are compared to those found with THz measurements.

3.3.1. Parameters of a Solar Cell

3.3.1.1. IV Curve

IV curve is the most important parameter in order to characterize a solar cell. The superposition of the IV curve of the diode in the dark and the light generated current gives the IV curve of the solar cell. Illuminating the solar cell causes shifting of the IV curve of the device in the light down to the fourth quadrant. The new ideal diode law with light generated current becomes [29]

$$I = I_0 \left[\exp\left(\frac{qV}{nkT}\right) - 1 \right] - I_L \quad (3.15)$$

Where I is the diode current, I_0 is the saturation current, q is the charge of an electron, V is the voltage across the diode, n is the ideality factor, k is the Boltzmann constant, T is the temperature and I_L is the light generated current. Without any illumination, a solar cell behaves like a diode in figure 3.9.

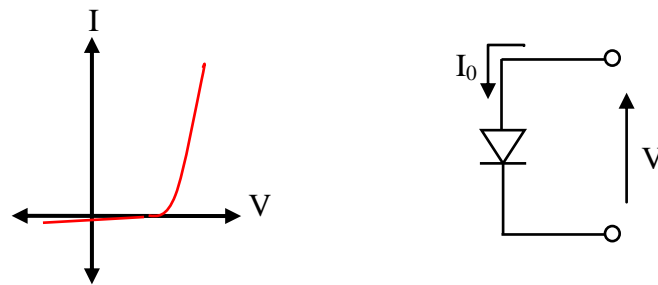


Figure 3.9: Without any illumination, a solar cell has the same electrical characteristics with a diode.

As the light is incident on the solar, IV curve shifts to the fourth quadrant in the figure 3.10 below and as the intensity increases the shift amount of the IV curve increase in figure 3.11.

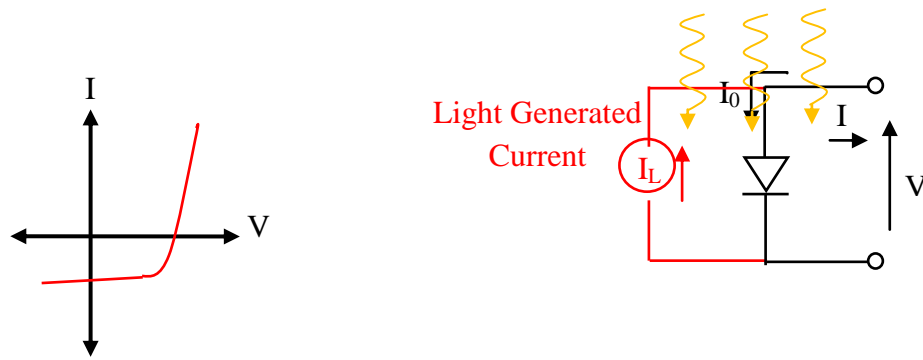


Figure 3.10: The incident light on the solar cell causes the shifting of the IV curve to the fourth quadrant

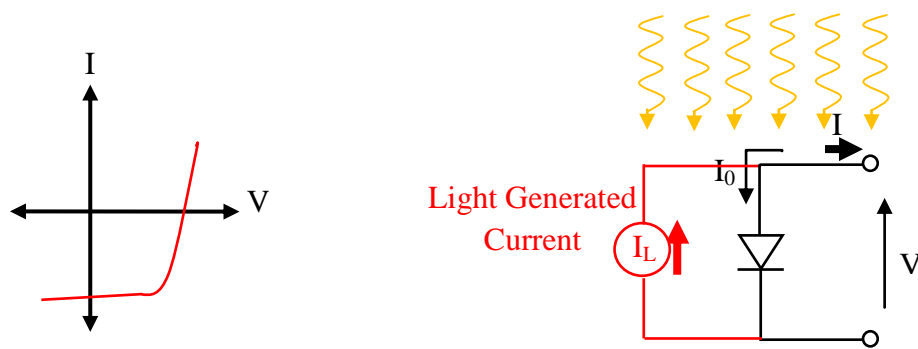


Figure 3.11: As the intensity of the incident light on the solar cell increases, the amount of the shift of the curve becomes greater

3.3.1.2. Short Circuit Current

When the solar cell is short circuited (or the voltage across the solar cell is zero), the current through the solar cell is the short circuit current, I_{sc} . The generation and collection of light generated carriers affect the short circuit current. In order to calculate the short circuit current, the photon flux should be known. This can be

calculated from the energy of the incident sunlight divided by the energy of one photon. Incident sunlight consists of different wavelength so; integrating these distributions from the lower wavelength to the upper wavelength at which electron-hole pairs are generated in the semiconductor, maximum short circuit current is obtained. The short circuit current depends on the area of the solar cell, the number of photons in the incident light, the spectrum of the incident light, the optical properties and the collection probability of the solar cell. The area of the solar cell also can be eliminated by using the short current density which is equal to the current per unit area rather than the short circuit current

Moreover, diffusion length is a significant parameter while comparing the solar cells. With uniform generation, the short circuit current density is written as

$$I_{sc} = qG(L_n + L_p) \quad (3.16)$$

Where G is the generation rate, L_n and L_p are the electron and hole diffusion lengths, respectively. As the band gap energy decreases, the short circuit current density increases, therefore, more photons create electron-hole pairs in the semiconductor [30].

3.3.1.3. Open Circuit Voltage

On the other hand, when the current through the solar cell is zero, the maximum voltage that is obtained is the open circuit voltage, V_{oc} . Also, the amount of forward bias on the solar cell gives the open circuit voltage and can be obtained form

$$V_{oc} = \frac{nkT}{q} \ln \left(\frac{I_L}{I_0} + 1 \right) \quad (3.17)$$

Light generated current, I_L and the saturation current, I_0 affect the amount of open circuit voltage. Saturation current, I_0 is related to the recombination on the solar cell. Then, the open circuit voltage depends on the recombination in the device [32].

3.3.1.4. Fill Factor

As mentioned before, the open circuit voltage and the short circuit current are the maximum voltage and the current that are obtained from the solar cell. However, at these points, the power that are delivered form the solar cell is zero. The fill factor, FF is the ratio of the maximum power from the solar cell to the product of open circuit voltage and the short circuit current. FF is most commonly defined as the largest rectangular area under the IV curve [36].

$$FF = \frac{I_{@ \max \text{ pow.}} V_{@ \max \text{ pow.}}}{I_{sc} V_{oc}} \quad (3.18)$$

FF is the fill factor, I_{sc} is the short circuit current and V_{oc} is the open circuit voltage. The maximum theoretical FF can be obtained by equalizing the derivative of the power from the solar with respect to voltage.

$$\frac{d(IV)}{dV} = 0 \quad (3.19)$$

Then, the voltage at maximum power is solved by the equation

$$V_{MP} = V_{oc} - \frac{nkT}{q} \ln \left(\frac{V_{MP}}{nkT/q} + 1 \right) \quad (3.20)$$

V_{MP} is the voltage at maximum power, n is the ideality factor, k is the Boltzmann constant, T is the temperature and q is the charge of one electron. According to this equation, n -factor is an important parameter in determining voltage. The junction quality and recombination type affect n -factor and change between 1 and 2.

The relationship between fill factor and open circuit voltage is written as [28]

$$FF = \frac{V_{oc} - \ln(V_{oc} + 0.72)}{V_{oc} + 1} \quad (3.21)$$

3.3.1.5. Solar Cell Efficiency

The performance of a solar cell is determined by the efficiency. The ratio of the energy output from the solar cell to input energy from the incident light gives the efficiency. Intensity and spectrum of the incident light and the temperature of the solar cell determines the efficiency. The efficiency of the solar cell is given by [28]

$$\eta = \frac{V_{oc} I_{sc} FF}{P_{in}} \quad (3.22)$$

Where $P_{max} = V_{oc} I_{sc} FF$, V_{oc} and I_{sc} are the open circuit voltage and short circuit current, respectively, FF is the fill factor and η is the efficiency. Energy conversion efficiencies of silicon solar cells is between 14% and 16%.

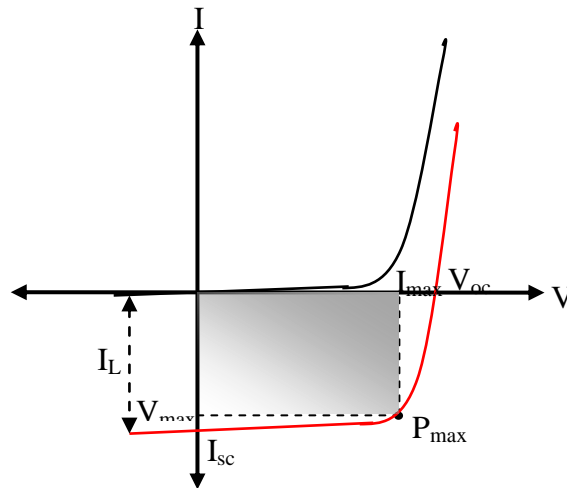


Figure 3.12: Typical IV Curve

From the above graph, open circuit voltage, V_{OC} , short circuit current, I_{SC} , maximum voltage, V_{max} , and maximum current, I_{max} are calculated from the IV curve under illumination. Open circuit voltage, V_{OC} , is determined where current, I , is zero and short circuit current, I_{SC} , is determined where voltage, V , is zero on the IV curve under illumination. Maximum voltage, V_{max} , and maximum current, I_{max} , are obtained from the biggest square that can be drawn between the IV curve under illumination and xy axes.

3.4. EFFECT OF TEMPERATURE

Solar cells are sensitive to temperature. As the temperature increases, the band gap energy of the semiconductor decreases. Therefore, the temperature affects most of the parameters of the solar cell. Moreover, the light intensity incident on the device affects the solar cell parameters like open circuit voltage, short circuit current, fill factor and the efficiency [26].

A semiconductor in which the highest energy levels for electrons i.e. the valence band is almost totally occupied. An intrinsic semiconductor is in which the free electrons in the conduction band and free holes in the valence band thermally excites through the semiconductor. An extrinsic semiconductor is in which additional electrons and holes exist in the conduction and valence band, respectively.

3.5. DISCUSSION

Using the above parameters and methods, the efficiency of the solar cell manufactured at METU MEMS is calculated in the next chapter. The solar cell we used in the measurements in this thesis has a thickness of 0.45 mm and is produced by the single silicon crystal in <100> direction. It is made up of a p-type base and n-

type emitter to create p-n junction. Also, it has a Si_3N_4 AR coating and Al back contacts as shown in the figure below.

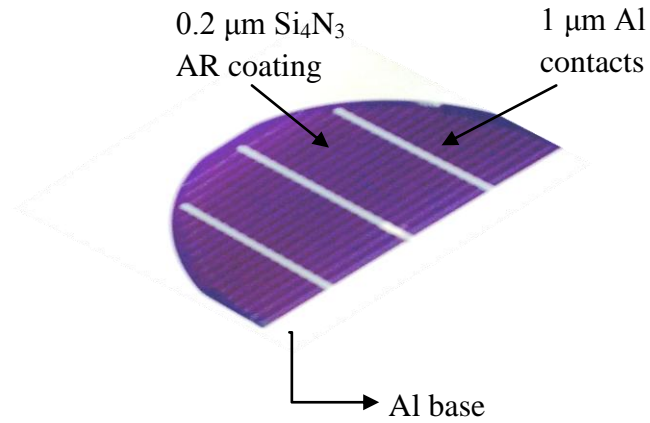


Figure 3.13: Single crystal silicon <100> solar cell

Our sample has an energy band gap 1.11 eV and a laser source with 808 nm wavelength was used in order to investigate its solar cell characteristics. The energy of one photon at 808 nm is approximately 1.53 eV, and it is higher than the energy band gap value. Therefore, charge carriers are excited from valence band to the conduction band. Due to the excitation of carriers, the efficiency of the solar cell is calculated in two methods explained in the next chapter.

CHAPTER 4

MEASUREMENTS OF THE SOLAR CELL

In this chapter, the efficiency of the solar cell was calculated with electrical methods and results were compared to the changes observed with THz-TDRS. In the first method, THz profiles of the solar cell were obtained with and without illumination. The differences in the change in the peaks of THz pulses are due to free-carriers which is an indication of the electrical response of the solar cell. In the second method, the IV curves of the solar cell under dark field and illumination were calculated. Then, with a classical current-voltage characteristics and parameters that are explained in the previous chapter, the efficiency of the solar cell was calculated.

4.1 THz MEASUREMENTS

The solar cell that is described in chapter 3.5 is used for the experiment. The solar cell has an area of 36.9 cm^2 . The solar cell can only be measured with reflection spectroscopy since it is opaque to THz radiation.

4.1.1. Experimental Procedure

The experimental set-up and how the THz-TDRS system works were explained in chapter 2. In addition, a diode laser which has a wavelength of 808 nm is placed into the system as shown in the figure 4.1 (with arrow). Then, the optical pulse from the

diode laser is directed to the solar cell with a mirror and focused with a lens which has a 40 cm focal length on the solar cell. The diameter of the optical pulse from the diode laser on the iris was about 1 cm. An iris was placed in front of the solar cell and the iris opening was adjusted to 5 mm. Moreover, the spot size of the THz radiation was calculated as 6 mm from chapter 2 section 2.4.1. The focal length of the lens was chosen in order to adjust the focus of the 808 nm laser beam on the solar cell with respect to the iris opening. Two types of measurements were taken with and without 808 nm diode laser illumination which has a power of 450 mW.

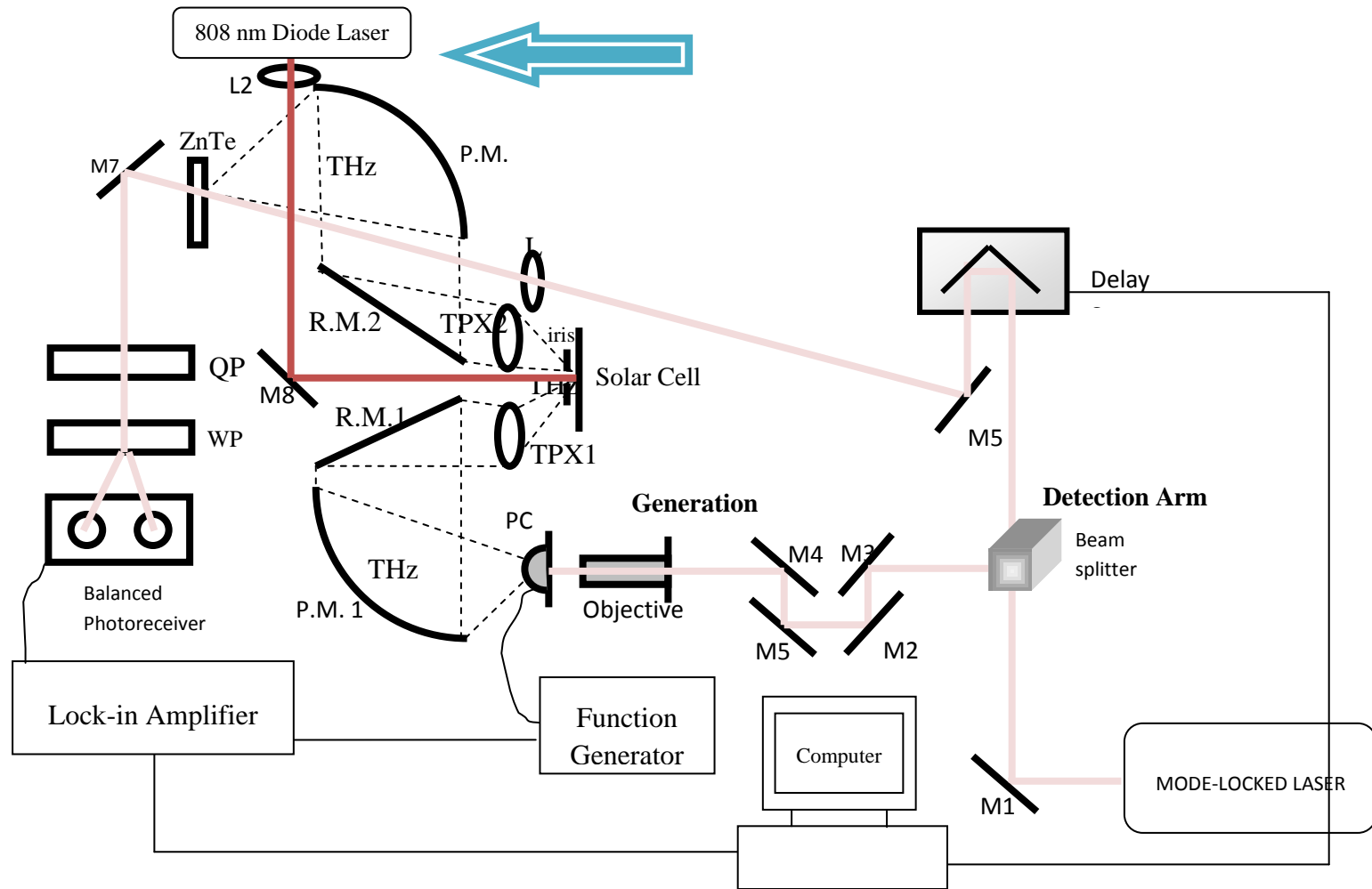


Figure 4.1: Experimental set-up with the addition of Diode Laser

4.1.2. Measurements of the Solar Cell by Using THz-TDRS

The two THz waveforms of the solar cell were compared in order to make the efficiency calculation as shown in the figure 4.4.

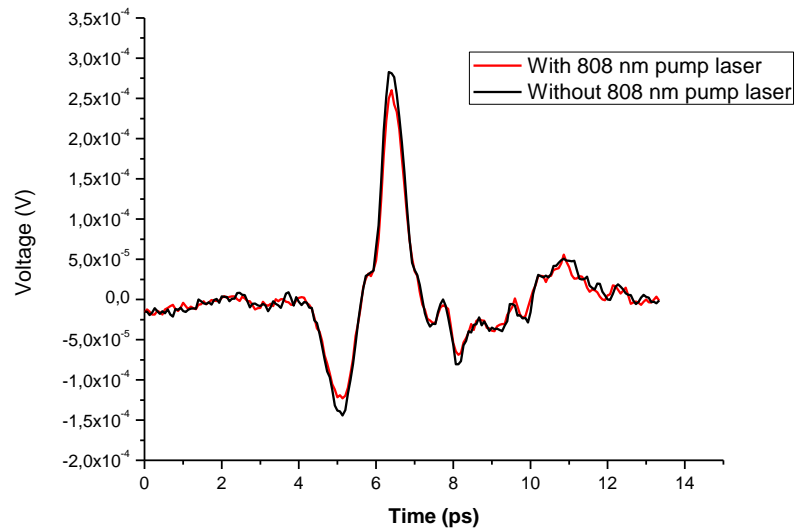


Figure 4.2: The comparison of THz profiles of the solar cell

Table 4.1: Peak-to-Peak voltages of THz Measurements with and without illumination

	Peak to Peak Voltage
With 808 nm diode laser illumination	$3.92 \times 10^{-4} \text{ V}$
Without illumination	$4.25 \times 10^{-4} \text{ V}$

As explained in the previous chapter, quantum efficiency of a solar cell can be determined by the ratio of the number of carriers collected by the solar cell to the

number of photons incident on the solar cell. However, in order to accurately say that the change in the peak we observe is an indication of quantum efficiency we need to perform further measurements at varying pump powers and actually verify the ratio of generated free-carriers to applied illumination power. Due to the figure shown above, it is assumed that there could be two reasons for the loss in the reflection peak. The first reason is that by applying laser pump to the solar cell, electrons are excited from valence band to the conduction band. At the same time, if THz is also incident, the electrons are excited in the intraband of the conduction band. The excitation of the electrons in the intraband causes the absorption of THz which results in the decrease in the amplitude of the THz pulse. The second reason is that, with the incident optical pulse and THz radiation, the refractive index of the solar cell is changed which causes the change in the reflection peak. This loss in the THz peak can be related to the number of free carriers in the solar cell. By doing more measurements under different powers, the change in the THz reflection peak can be observed more precisely. If the ratio of the THz peaks with and without varying applied power in illumination changes linearly with applied power then we can argue that the THz measurements can give an approximation for the quantum efficiency of the solar cell. However, in order to say this, the dynamics of the recombination and generation of free-carriers under external illumination has to be well understood. The only conclusion that can be drawn from our results is that in this measurement as shown in the figure above, the ratio of the difference of the THz pulse peak to peak voltage amplitude to the THz pulse peak to peak voltage amplitude without illumination gives a percent loss of the reflected THz intensity which is an indicator of the number of free-carriers generated in the solar cell and this value corresponds to 7.7 %. The error in this measurement is dependent on the system signal to noise ratio which is about 100:1.

4.2. ELECTRICAL MEASUREMENTS

4.2.1. Experimental Procedure

The electrical characterization measurements on the solar cell were performed by using two techniques: Solar Cell Simulator and 808 nm Diode laser. These electrical measurements were done in order to calculate the efficiency of the solar cell in a different method and compare the results with THz measurements.

The solar cell simulator is a device that measures the efficiency by illuminating the solar cell. The intensity of incident light on the solar cell is measured by the number of suns. 1 sun is equal to 1 kW/m^2 . In our case, the intensity of incident light in the solar simulator is 0.6 sun. The contacts of the solar cell were connected to current-voltage source named Keithley 2400 sourcemeter. Then, IV curve of the solar cell under illumination is obtained by the sourcemeter controlled by the computer program. The efficiency of the solar cell was measured as 4.8 % under 0.6 sun.

Apart from this; the other electrical measurements were taken by placing the solar cell back in the THz-TDRS system where it was illuminated by the 808nm diode laser with 450 mW power. The contacts of the solar cell in the system were connected to the same sourcemeter and electrical measurements were obtained with the help of the sourcemeter controlled by the computer. Two different combinations of measurements were done. One of them is made without any illumination and the other measurement was made by illuminating the solar cell with 808 nm laser pump while at the THz peak. The second measurement was taken to ensure that the THz field does not affect the measurements. The I-V measurements were done at room temperature and the source voltage was varied between -2 and 2 voltage range with 0.1 V step size.

First, the dark IV curve (no illumination and no THz) of the solar cell was obtained in order to observe the shift of the curve when taken under illumination. Second, IV curve under THz radiation only was obtained. It is observed that both the dark IV

curves and the THz IV Curve is very similar as shown in the figure 4.3 since only THz radiation does not make any change in the carriers on the solar cell.

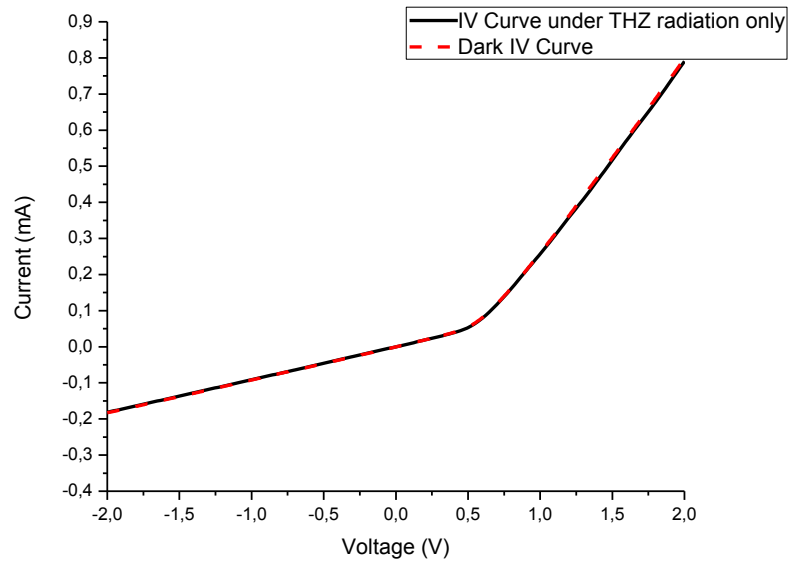


Figure 4.3: IV Curve under dark field and illumination with THz radiation only

Then, 808 nm laser pump only was obtained and shown in the figure 4.4.

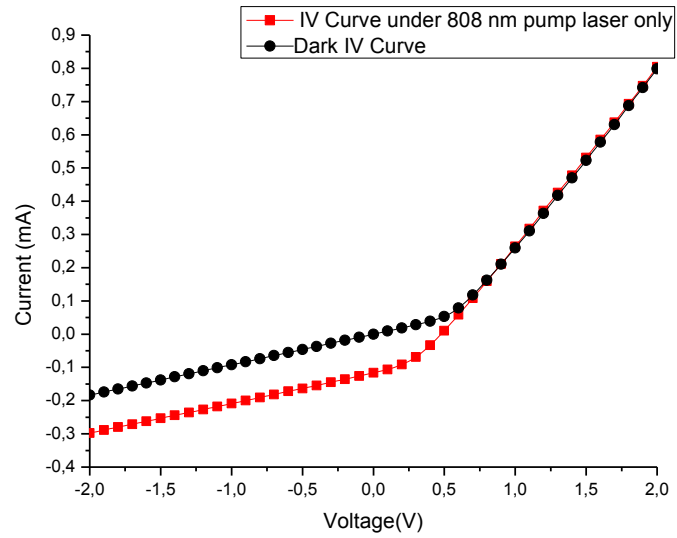


Figure 4.4: IV Curve under dark field and illumination with 808 nm laser only

Third, IV curve under 808 nm laser pump with THz radiation was obtained and shown in the figure 4.5.

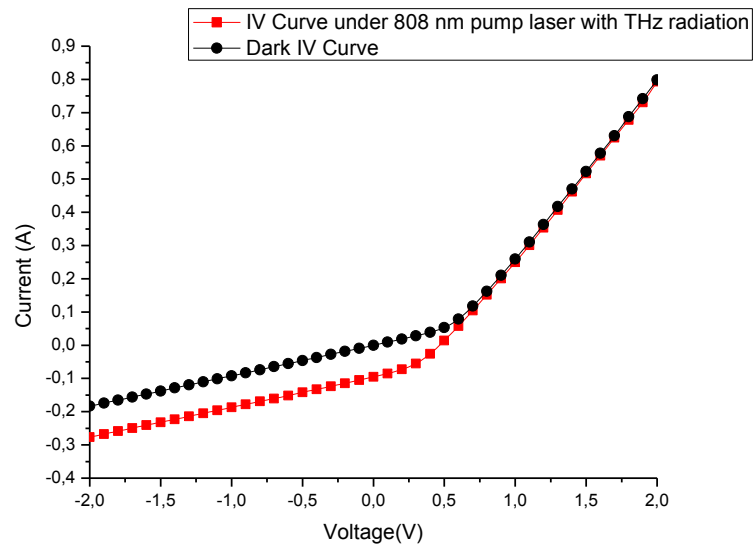


Figure 4.5: IV Curve under dark field and illumination with 808 nm laser and THz radiation

4.2.2. Efficiency Calculation of the Solar Cell by Using Electrical Measurements

As mentioned in the previous chapter, the efficiency of a solar cell by using an ideal current-voltage characteristic of a solar cell under dark field and illumination can be calculated. With the same calculation method, the open circuit voltage V_{OC} and the short circuit current I_{SC} of the solar cell was found to be 0.50 V and 0.11 A (the method of obtaining these values were explained in chapter 3 section 3.1.5.), respectively. Moreover, for the maximum power (the method of calculation was explained in chapter 3 section 3.1.5.), the maximum voltage, V_{max} , and the maximum current, I_{max} , was obtained 0.31 V and 0.05 A, respectively. Afterwards we calculate the fill factor, FF, given by equation 3.18 where the short circuit current, I_{SC} , is 0.11 A, the open circuit voltage, V_{OC} , is 0.50 V and .), the maximum voltage, V_{max} , and the maximum current, I_{max} , is 0.31 V and 0.05 A, respectively. From here the efficiency is given by equation 3.22. Using these equations, the efficiency of the solar cell was calculated to be 3.44% in the electrical measurements.

Furthermore, External Quantum Efficiency is also used to represent the efficiency of a solar cell in converting light power to electrical power. This can be calculated from the equation below.

$$Q_E = \frac{\text{\# of carriers collected by the solar cell}}{\text{\# of photons of a given energy}} = \frac{\frac{\text{Current Measured}}{\text{Charge of one electron}}}{\frac{\text{Total power of photons}}{\text{Energy of one photon}}} \quad (4.1)$$

Where the current measured under illumination was 0.02 A. The charge of one electron is $1.62 \times 10^{-19} C$, total power is 450 mW and energy of one photon is $2.46 \times 10^{-19} J$. Using these values the external quantum efficiency for our solar cell is

$$Q_E \approx 7 \% \quad (4.2)$$

CHAPTER 5

CONCLUSION

In this thesis, a compact THz-TDRS was designed and constructed. Since the samples that were observed in this thesis were opaque to the THz radiation, the system was built for reflection spectroscopy. Photoconductive antenna was used in the generation and electro-optic crystal was used in detection of THz radiation.

To determine whether this type of system can be used to characterize solar cells first an un-doped silicon wafer was tested under illumination and without illumination in the system. A diode laser with a wavelength 808 nm and average power of 450mW was used to illuminate the samples. Areas that were illuminated were 6 mm for both the silicon wafer and the solar cell. THz waveforms were obtained under the illumination of the diode laser and without any illumination. Then, the two waveforms were compared and loss in the THz peak amplitude that was taken under illumination with respect to the measurement without illumination was observed. One of the possible results for the loss in the THz reflection peak is that as the optical pulse (coming from 808 nm Diode Laser) is incident on the silicon wafer, the carriers are excited from valence band to conduction band. Moreover, as THz strikes to the silicon wafer, the carriers move in the intraband causing the absorption of THz wave. Therefore, the reflection amplitude from the silicon wafer is decreased due to this absorption. The other possible reason why there is a loss in the reflection peak is the change in the refractive index of the solar cell while it is illuminated with both THz and the external source. Moreover, by doing more measurements under different powers, the change in the THz reflection peak can be observed more precisely.

Generally, quantum efficiency of a solar cell can be determined by the ratio of the number of carriers collected by the solar cell to the number of photons incident on the solar cell. However, further measurements should be done in order to accurately say that the change in the peak we observe is an indication of quantum efficiency. Therefore, we need to perform further measurements at different pump powers. If the ratio of the THz peaks with and without different applied power in illumination changes linearly with the applied power then we can argue that the THz measurements can give an approximation for the quantum efficiency of the solar cell.

A solar cell obtained from METU-MEMS had a 0.45 mm thickness. It was made up of p-type base and n-type emitter with Si_3N_4 AR coating and Al back contacts. Similar measurements were done on the solar cell as in the silicon wafer sample and the same response was observed with and without illumination. Then, by using these THz measurements, we extrapolated the change in the THz peak reflection and this change is related to the free carrier number in the solar cell. Both the absorption of THz radiation in the solar cell and the change in the refractive index of the solar cell results this change in the THz reflection peak. If the loss in the peak scales linearly with the excitation power, and we can conclude that changing the excitation power changes the number of free-carriers in the solar cell linearly, then, the quantum efficiency of the solar cell would be about 7.7% (error is about 1%) as observed in the THz measurements. In the course of these measurements theoretical background on the electrical working principles were given for the solar cells. These solar cell parameters were used in order to calculate the external quantum efficiencies and energy conversion efficiencies using well established electrical techniques as outlined in the next paragraph.

To compare with THz measurements electrical contact measurements on the solar cell were also done. IV curves were obtained using the electrical contacts on the solar cell under 808nm diode laser illumination of about 450mW. By using the results of the measurements, theoretical calculations were done for the external quantum efficiency. In order to obtain typical IV curve of the solar cell, electrical measurements were done in the dark (without any illumination), under illumination

and under illumination with THz radiation. Since, THz radiation has a low energy when compared with the energy band gap of the silicon, the excitation of the carriers from band to band transitions does not occur. IV measurements show that the results obtained in the illumination with diode laser only and those with THz radiation are nearly the same as expected. The external quantum efficiency calculated by these electrical contact methods give a value of 7% (error is small and negligible) at this particular illumination wavelength.

In conclusion, more comprehensive measurements should be done in order to understand the dynamics of the recombination and generation of free-carriers under external illumination. In this experiment, the most important result is that the ratio of the difference of the THz pulse peak to peak voltage amplitude to the THz pulse peak to peak voltage amplitude without any illumination gives a percent loss of the reflected THz intensity.

In the future THz-TDRS systems can be developed to scan the surface of a solar cell and obtain the efficiency and/or electrical characteristics thereby providing the solar cell industry a valuable tool that can make these important measurements without actually touching or making contacts with the solar cell. For future work, THz measurements on the solar cells are planned to be translated into THz images of the solar cell by placing the solar cells on xyz scanning stages.

REFERENCES

- [1] Dexheimer, S. L. Terahertz Spectroscopy: Principles and Applications; CRC Press: Boca Raton, 2007.
- [2] R. A. Cheville, "Terahertz Time-Domain Spectroscopy with Photoconductive Antenna".
- [3] S. Verghese, K. A. McIntosh, E. R. Brown: IEEE Trans. Microwave Th. Tech. 45, 1301 (1997).
- [4] B. B. Hu, X. -C. Zhang, D. H. Auston: "Terahertz radiation induced by sub-bandgap femtosecond optical excitation of GaAs", Phys. Rev. Lett. 67, 2709 (1991).
- [5] D. M. Mittleman, M. Gupta, R. Neelamani, R. G. Baraniuk, J. V. Rudd, M. Koch: Recent Advances in Terahertz Imaging, App. Phys. B, V. 68, I. 6, pp. 1085-1094 (1999).
- [6] Keiding, S. R. J. Phys. Chem. A 1997, 101, 5250-5254.
- [7] Knoesel, E.; Bonn, M.; Shan, H.; Heinz, "Charge transport and carrier dynamics in liquids probed by THz-Time Domain Spectroscopy", T. F. Phys. Rev. Lett. 2001, 86, 340.
- [8] Markelz, A. G.; Roitberg, A.; Heilweil, E. J. Chem. Phys. Lett. 2000, 320, 42- 48.
- [9] Dragoman, D.; Dragoman, M. Progress in Quantum Electronics 2004, 28, 1-66.
- [10] Davies, A. G.; Linfield, E. H.; Johnston, "The development of terahertz sources and their applications", M. B., Phys. Med. Biol. 47 (2002) 3679-3689.
- [11] Beard, M. C.; Turner, G. M.; Schmuttenmaer, "Transient Photoconductivity in Dye-Sensitized Nanocrystalline TiO₂ Films as Measured by Time-Resolved THz Spectroscopy", C. A. J. Phys. Chem. A, 2002, 106, 878-883
- [12] D. Mittleman, Ed., Sensing with Terahertz Radiation. Berlin: Springer, 2002.

- [13] J. D. Wai Lam Chan and D. M. Mittleman, "Imaging with terahertz radiation," *Rep. Prog. Phys.*, vol. 70, p. 1325, 2007.
- [14] K. Yang, P. Richards, and Y. Shen, "Generation of far-infrared radiation by picosecond light pulses in linbo₃," *Appl. Phys. Lett.*, vol. 19, p. 320, 1971.
- [15] M. V. Exter, Ch. Fattinger, and D. Grischkowsky, "High- brightness terahertz beams charecterized with an ultrafast detector" *Appl. Phys. Lett.* **55**, 4, 337-339 (1989).
- [16] Y. R. Shen, "Far-infrared generation by optical mixing," *Prog. Quant. Electron.*, vol. 4, p. 207, 1976.
- [17] D. Auston and K. Cheung, "Coherent time-domain far-infrared spectroscopy," *J. Opt. Soc. Am. B*, vol. 2, pp. 606–612, 1985.
- [18] P. Smith, D. Auston, and M. Nuss, "Subpicosecond photoconducting dipole antennas," *IEEE J. Quant. Elect.*, vol. 24, no. 2, pp. 255–260, 1988.
- [19] Q. Wu and X. Zhang, "Free-space electro-optic sampling of terahertz beams," *Appl. Phys. Lett.*, vol. 67, p. 3523, 1995.
- [20] B. Hu and M. Nuss, "Imaging with terahertz waves," *Opt. Lett.*, vol. 20, no. 16, pp. 1716–1718, 1995.
- [21] *J. Scott Moore*, "New wave: Terahertz radiation will soon open new doors for manufacturers", <<http://www.automationmag.com/magazine/content/manufacturing-trends/new-wave-terahertz-radiation-will-soon-open-new-doors-for-manufacturers.html>>, posted 22.07.2010.
- [22] B. Ferguson and X. Zhang, "Materials for terahertz science and technology," *Nat. Mater.*, vol. 1, no. 1, pp. 26–33, 2002.
- [23] Ohba T and Ikawa S, "Far-infrared absorption of silicon crystals", 1988 *J. Appl. Phys.* 64 4141.
- [24] Van Exter M and Grishkowsky D 1990 *Appl. Phys. Lett.* 36 1694.
- [25] Nagai, N., Sumitomo, M., Imaizumi, M., & Fukasawa R. Characterization of electron- or proton-irradiated Si space solar cells by THz spectroscopy, *Semicond. Sci. Technol.* 21, 201-209, 2006.
- [26] Hashimshony, D., Geltner, I., Cohen, G., Avitzour, Y., Zigler, A., Smith, C., *Journal of Applied Physics*, Volume 90, Issue 11, pp. 5778-5781 (2001).
- [27] Reddy, P. J. *Science and Technology of Photovoltaics*; CRC Press 2010.

- [28] Partain, L. D. Solar Cells and Their Applications; John Wiley& Sons: USA, 1995.
- [29] Fahrenbruch, A. L.; Bube, R. H. Fundamentals of Solar Cells: photovoltaic Solar Energy Conversion; Academic Press, 1983.
- [30] Würfel, P. Physics of Solar Cells: From Basic Principles to Expanded Edition Wiley 2009.
- [31] Goetzberger, A., Luther, J., and Willeke, G., Solar Energy Materials & Solar Cells 74 (2002)
- [32] Fattinger, C.; Grischkowsky, “Terahertz Beams”, D. Appl. Phys. Lett. 1989, 54, 490-492
- [33] Vaan Exter, M; Fattinger, C, Grischkowsky, D. Appl. Phys. Lett. 1989, 55, 337-339.
- [34] Wengenmayr, R.; Bürke, T. Renewable Energy: Sustainable Concepts for the Future; Wiley, 2008.
- [35] Nelson, J., the Physics of Solar Cells, Imperial College Press, 2003.
- [36] Smestad, G. P., Optoelectronics of Solar Cell, Spie Press, 2002.
- [37] Green, M. A., Solar Cells: Operating Principles, Technology and system applications, Prentice Hall, 1982.
- [38] Lee, Y. S., Principles of Terahertz Science and Technology, Springer, 2009.
- [39] Thorlabs, <http://www.thorlabs.com/catalogpages/v20/706.pdf>, last visited January 2011.
- [40] Batop http://www.batop.de/products/photoconductive-antenna/data-sheet/manual_PCA-44-06-10-1030.pdf, last visited January 2011.
- [41] CVI Melles Griot
<http://www.cvimellesgriot.com/Products/Documents/Catalog/POA.pdf>, last visited January 2011.
- [42] Stanford Research Systems,
<http://www.thinksrs.com/downloads/PDFs/Manuals/SR830m.pdf>, last visited January 2011.

- [43] M. Naftaly, R. E. Miles, *Member, IEEE* and P. J. Greenslade, THz Transmission in Polymer Materials –a Data Library.
- [44] P. C. M. Planken, H.-K. Nienhuys, H. J. Bakker and T. Wenckebach “Measurement and calculation of the orientation dependence of terahertz pulse detection in ZnTe” *J. Opt. Soc. Am. B* **18**, 3, 313-317 (2001).
- [45] J. C. Wiltse, “History of millimeter and submillimeter waves” *IEEE Trans. On Microwave Theo. and Thec.* **32**, 9 (1984).
- [46] Q. Wu and X.-C. Zhang, “Free-space electro-optic sampling of terahertz beams” *Appl. Phys. Lett.* **67**, 24, 3523- 3525 (1995).
- [47] A. Nahata, A. S. Weling, and T. F. Heinz, “A wideband coherent terahertz spectroscopy system using optical rectification and electro-optic sampling” *Appl. Phys. Lett.* **69**, 16, 2321-2323 (1996).
- [48] K. Sakai, and M. Tani, “Introduction to Terahertz Pulses” *K. Sakai (Ed.): Terahertz Optoelectronics, Topics Appl. Phys.*, **97**, 1-30 (2005).